THE STUDY ABOUT FINITE ELEMENT ANALYSIS OF DEGRADATION MG ALLOY FOR BIOMEDICAL IMPLANT

2023
MASTER THESIS
METALLURGICAL AND MATERIALS ENGINEERING

Bupe KASANYA

Thesis Advisors
Assist. Prof. Dr. Ismail Hakkı KARA
Assist. Prof. Dr. Ramazan ÖZMEN

THE STUDY ABOUT FINITE ELEMENT ANALYSIS OF DEGRADATION MG ALLOY FOR BIOMEDICAL IMPLANT

Bupe KASANYA

Thesis Advisors

Assist. Prof. Dr. Ismail Hakkı KARA

Assist. Prof. Dr. Ramazan ÖZMEN

T.C.

Karabuk University

Institute of Graduate Programs

Department of Metallurgical and Materials Engineering

Prepared as

Master Thesis

KARABUK

August 2023

I certify that in my opinion the thesis submitted by Bupe KASANYA titled "THE STUDY ABOUT FINITE ELEMENT ANALYSIS OF DEGRADATION MG ALLOY FOR BIOMEDICAL IMPLANT" is fully adequate in scope and in quality as a thesis for the degree of Master of Science.

Assist. Prof. Dr. Ismail Hakkı KARA .....
Thesis Advisor, Department of Metallurgical and Materials Engineering

Assist. Prof. Dr. Ramazan ÖZMEN .....
Thesis Advisor, Department of Mechatronics Engineering

This thesis is accepted by the examining committee with a unanimous vote in the Department of Metallurgical and Materials Engineering as a Master of Science thesis. 10/08/2023

Examining Committee Members (Institutions)	Signature
Chairman : Prof. Dr. Mustafa ACARER (SU)	.....
Member : Prof. Dr. Hayrettin AHLATCI (KBU)	.....
Member : Assist. Prof. Dr. İsmail Hakkı KARA (KBU)	.....

The degree of Master of Science by the thesis submitted is approved by the Administrative Board of the Institute of Graduate Programs, Karabuk University.

Prof. Dr. Müslüm KUZU .....
Director of the Institute of Graduate Programs

"I declare that all the information within this thesis has been gathered and presented in accordance with academic regulations and ethical principles and I have according to the requirements of these regulations and principles cited all those which do not originate in this work as well."

Bupe KASANYA

ABSTRACT

M. Sc. Thesis

THE STUDY ABOUT FINITE ELEMENT ANALYSIS OF DEGRADATION MG ALLOY FOR BIOMEDICAL IMPLANT

Bupe KASANYA

Karabuk University
Institute of Graduate Programs
The Department of Metallurgical and Materials Engineering

Thesis Advisors:
Assist. Prof. Dr. Ismail Hakkı KARA
Assist. Prof. Dr. Ramazan ÖZMEN
August 2023, 61 pages

The increasing demand for biodegradable and biocompatible metallic materials in medical applications has led to extensive research on the use of magnesium (Mg) and its alloys (Mg alloys) as potential candidates for implantable devices. What makes magnesium and its alloys potential candidates for use as biodegradable metallic materials are their unique biocompatibility and biodegradability advantages over traditional metallic biomaterials such as titanium alloys, stainless steel, cobalt-chromium based alloys etc. However, the corrosion behaviour of magnesium and its alloys remains a critical concern that hinders their widespread implementation in the medical fraternity. AT31 magnesium alloy (Mg-2.5Al-1.0Sn-0.3Mn-0.4La-1.33Gd) produced by casting is used in this thesis. The alloy was homogenised at 350°C and hot rolling was performed at three different temperatures, 350°C, 400°C, and 500°C, to deform the alloy from 5 mm to 3.5 mm, 4.0 mm, and 4.5 mm thicknesses, thus

resulting in three different sample classification (Mg350s, Mg400s, and Mg500s respectively). During hot rolling, the thickness deformation rates were 30%, 20%, and 10% respectively. Corrosion experimental procedures were performed to investigate the corrosion performance of each alloy. The electrochemical parameters obtained from the experiments such as corrosion current (I_{corr}), corrosion potential (E_{corr}) etc., were used in the computation modelling and simulation of the corrosion process of the various magnesium samples.

Comprehensive models are developed to simulate the corrosion process and performance of the magnesium alloy implants under physiological conditions in COMSOL Multiphysics. Finite element techniques are used to solve complex partial differential equations (PDEs) of a given model in COMSOL Multiphysics.

The aim of this thesis is to compare three magnesium alloys – AT31 magnesium alloys, regarding their corrosion resistance in a physiological environment as well as evaluate the effectiveness of the simulation methods for verifying the experimental findings related to the corrosion performance of these magnesium alloys.

Keywords : Magnesium, magnesium alloy, corrosion, biocompatibility, potentiodynamic polarisation, simulation.

Science Code : 91501

ÖZET

Yüksek Lisans Tezi

BIYOMEDIKAL IMPLANT IÇIN BOZUNMA MG ALAŞIMININ SONLU ELEMAN ANALIZI ILE ILGILI ÇALIŞMA

Bupe KASANYA

Karabük Üniversitesi
Lisansüstü Eğitimi Enstitüsü
Metalurji ve Malzeme Mühendisliği Anabilim Dalı

Tez Danışmanları:
Dr. Öğr. Üyesi Ismail Hakkı KARA
Dr. Öğr. Üyesi Ramazan ÖZMEN
Ağustos 2023, 61 sayfa

Tıbbi uygulamalarda biyolojik olarak parçalanabilen ve biyouyumlu metalik malzemelere yönelik artan talep, magnezyum (Mg) ve alaşımlarının (Mg alaşımları) implante edilebilir cihazlar için potansiyel adaylar olarak kullanımı konusunda kapsamlı araştırmalara yol açmıştır. Magnezyum ve alaşımlarını biyolojik olarak parçalanabilir metalik malzemeler olarak kullanım için potansiyel adaylar haline getiren şey, titanyum alaşımları, paslanmaz çelik, kobalt-krom bazlı alaşımlar gibi geleneksel metalik biyomalzemelere göre benzersiz biyouyumluluk ve biyolojik olarak parçalanabilirlik avantajlarıdır. Bununla birlikte, magnezyum ve alaşımlarının korozyon davranışı, tıp dünyasında yaygın olarak uygulanmalarını engelleyen kritik bir endişe kaynağı olmaya devam etmektedir. Bu tezde döküm yoluyla üretilen AT31 magnezyum alaşımı (Mg-2.5Al-1.0Sn-0.3Mn-0.4La-1.33Gd) kullanılmıştır. Alaşım 350°C'de homojenize edilmiş ve 350°C, 400°C ve 500°C olmak üzere üç farklı

sıcaklıkta sıcak haddeleme gerçekleştirilerek alaşım 5 mm'den 3,5 mm, 4,0 mm ve 4,5 mm kalınlıklara deforme edilmiş, böylece üç farklı numune sınıflandırması (sırasıyla Mg350s, Mg400s ve Mg500s) elde edilmiştir. Sıcak haddeleme sırasında kalınlık deformasyon oranları sırasıyla %30, %20 ve %10 olmuştur. Her bir alaşımın korozyon performansını araştırmak için korozyon deneysel prosedürleri gerçekleştirilmiştir. Deneylerden elde edilen korozyon akımı (I_{corr}), korozyon potansiyeli (E_{corr}) vb. elektrokimyasal parametreler, çeşitli magnezyum numunelerinin korozyon sürecinin hesaplama modellemesinde ve simülasyonunda kullanılmıştır.

COMSOL Multiphysics'te fizyolojik koşullar altında magnezyum alaşımlı implantların korozyon sürecini ve performansını simüle etmek için kapsamlı modeller geliştirilmiştir. COMSOL Multiphysics'te belirli bir modelin karmaşık kısmi diferansiyel denklemlerini (PDE'ler) çözmek için sonlu eleman teknikleri kullanılmıştır.

Bu tezin amacı, üç magnezyum alaşımını - AT31 magnezyum alaşımları, fizyolojik bir ortamda korozyon dirençleri açısından karşılaştırmak ve bu magnezyum alaşımlarının korozyon performansı ile ilgili deneysel bulguları doğrulamak için simülasyon yöntemlerinin etkinliğini değerlendirmektir.

Anahtar Kelimeler : Magnezyum, magnezyum alaşımı, korozyon, biyouyumluluk, potansiyodinamik polarizasyon, simülasyon.

Bilim Kodu **:** 91501

ACKNOWLEDGEMENTS

Primarily, I would like to acknowledge and give thanks to YAHWEH for guiding me and granting me strength throughout my master's study, especially towards the end, I almost throw in the towel and gave it all up but YAHWEH, the most High God, strengthened me. To my beloved relatives, friends, and workmates thank you for your unwavering love, understanding, and endless encouragement. To my mum and my girlfriend's mum, your unwavering love and unwavering support, built confidence within me, and your valuable insights, advice, and encouragement have been immensely valuable in keeping me focused and motivated. A special thanks goes to Polimak's General Manager Mr Süleyman SALIHLER and the entire Polimak staff for providing me with flexibility, resources, and unwavering support. Your understanding and support have made it possible for me to strike a balance between education and work.

To my supervisor, Assist. Prof. Dr. İsmail Hakkı KARA, I am deeply grateful for your guidance and expertise. Your constructive criticism and commitment to my academic development have been instrumental in shaping the direction and quality of this thesis. A special shout-out to Gary and Imran for always accommodating me in Karabük. To Bukie and Lungelo, you guys fully prepared me for my defence and for that, I will forever be grateful.

I would also like to express my heartfelt gratitude to my girlfriend, Bukelwa MAPHANGA, whose unwavering love, patience, and understanding have been an incredible source of inspiration. Your encouragement, constructive feedback, and willingness to lend a helping hand have played an integral role in shaping the outcome of this thesis. Thank you for standing by my side throughout this challenging journey. Finally, I would like to acknowledge myself with much gratitude for the dedication, hard work, and perseverance invested in this research. This thesis stands as a testament to my commitment to academic excellence and personal growth. I am proud of the

effort and determination I have put into this endeavour, and I am grateful for the lesson and growth it has brought me.

CONTENTS

Page

Page

Page

LIST OF FIGURES

Pages

LIST OF TABLES

Pages

SYMBOLS AND ABBREVIATIONS INDEX

SYMBOLS

Mg : Magnesium
Al : Aluminium
Sn : Tin
Mn : Manganese
La : Lanthanum
Gd : Gadolinium
Cl : Chlorine
Na : Sodium
NaCl : Sodium chloride
Mg^{2+} : Magnesium ion
H^{+} : Hydrogen ion
Cl^{-} : Chloride ion
Na^{+} : Sodium ion
R : Gas constant
F : Faraday's constant
c_i : Concentration of species *i*
D_i : Diffusion coefficient
u_{mi} : Mobility of species *i*
ρ : Density
η : Overpotential

ABBREVIATIONS

Icorr : Corrosion current
Ecorr : Corrosion potential
FEM : Finite Element Method

ASTM : American Society for Testing and Materials

K_{sp} : Solubility product

Q_{sp} : Reaction quotient

PART 1

INTRODUCTION

1.1. BRIEF DISCOVERY

Magnesium has a fascinating history that dates back several centuries. According to literature, the summer of 1816 saw England experience a period of drought and during this period, a farmer (cowherd) by the name of Henry Wicker came across a water source (well) in Epsom Common. Strangely, his thirty cattle refused to drink from it because the water tasted bitter and when the water evaporated, it produced a salt (Epsom salt) that had extraordinary properties. Epsom salt became popular over the following years. In 1965, Nehemiah Grew, an English plant atomist and physiologist, made a publishment in which the first significant light was shed on Epsom salt [1, 2]. The salt contained in Epsom was identified as magnesium sulphate ($MgSO_4$) and made its initial entry into medicine. N. Grew specifically demonstrated that it was possible to consume the salt without the need of taking considerable quantities of water.

In 1755, a proposition was made by Joseph Black of Edinburgh – a Scottish physicist and chemist, that magnesium was an element. He showed that magnesia (MgO) differed from lime (calcium oxide) even though both were produced by heating their respective carbonate ores [3]. By 1792, an impure form of metallic magnesium was produced by Anton Rupprecht by heating magnesia with charcoal. In 1808, Sir Humphrey Davy of London successfully identified magnesium for the first time by isolating it from a mixture of magnesium oxide and mercuric oxide [4, 5]. Further advancements were made in 1828 by the French chemist Antoine Alexandre Brutus Bussy, who obtained relatively pure magnesium by reducing anhydrous magnesium chloride with potassium [5]. Additionally, in 1833, the English scientist Michael Faraday FRS, an assistant to Sir Humphrey Davy, achieved the production of magnesium through the electrolysis of molten magnesium chloride, which remained

the primary industrial method until thermal processes such as carbothermic and ferrosilicon techniques were introduced [5].

1.2. BACKGROUND

With the medical fraternity not being an independent arena for a long time now, we see that medicine and engineering are not far apart. The influence and contribution the engineering fraternity has in this field can be evidently seen in the application of design concepts and principles for healthcare purposes. Cutting-edge orthopaedic surgical treatments greatly depend on the quality development of biomaterial used for fracture fixations and joint replacements. A biomaterial is simply a synthetic material used in medical applications such as orthopaedic, cardiovascular, and dental for the treatment and replacement of injured or damaged tissue [6]. In our everyday life, the human body may experience various injuries including fractures which are highly dependent on an individual's age, gender (male or female), bone strength, and overall health [7].

A large number of individuals experience bone fractures and degenerative joint diseases (also known as Osteoarthritis – OA) every single year, necessitating different treatments depending on the extent of the fracture and disease. Diseases such as degenerative joint diseases typically necessitate the replacement of damaged tissues with permanent implants like artificial knees and hips, thereby leaving the implant intact in the human body. To ensure durability within the body, most of these implants are engineered from inert materials like titanium alloys, stainless steel, cobalt-chromium-based alloys etc. Fracture fixation, on the other hand, may involve the surgical insertion of metallic pins, screws, and plates to externally support the affected bone tissue during the time of healing. In such cases, orthopaedic implants must be designed to only render support to the treated bone through its process of healing [8]. Literature shows that the most used materials for bone fixation are metallic materials like titanium alloys and stainless steel. However, because this type of injury is temporary and non-biodegradable metallic materials are used to provide support during the healing process of the tissue, a second surgery is required to remove the implant after full recuperation of the tissue. Not only is the procedure (second surgery) costly, but it may also lead to re-damaging of the healed tissue/bone as well as bring

discomfort to the patient. For temporary injuries, desirable temporary orthopaedic implants – biodegradable, would render adequate mechanical strength upon implantation, then gradually undergo degradation while being replaced by the fresh bone tissue as the patient recovers, thus no second surgery is needed. Some of the biodegradable implants are engineered from polymeric and ceramic materials like polylactide (PLA) and polyglycolide (PGA) [9, 10, 11, 12]. However, a significant setback of utilising polymers is their limited mechanical stability, which then leads to premature failure of the implant.

Over the years, the demand for biodegradable metallic implants has significantly increased due to some of the drawbacks associated with biodegradable polymeric implants and permanent metallic implants. Magnesium and its alloys have been considered as one of the potential options for metallic biodegradable material for medical implants. Literature shows that magnesium is a necessary nutrient that the human body needs to stay healthy. It is needed in the body for metabolism, biological mechanisms, and bone formation by stimulating osteoblast proliferation [12, 13]. Magnesium is the fourth most abundant cation in the human body with an estimated 1 mol (approximately 24.31 grams) of magnesium stored in the body of a 70 kg individual (adult) [14]. Moreover, magnesium possesses biocompatibility and biodegradability, its mechanical properties such as Young's modulus and specific density, are like that of the human bone [12]. Such unique properties of magnesium make it an excellent and attractive material for medical applications.

Magnesium is an exceptionally lightweight metal with a low density (1.738 g/cm^3) and high strength-to-weight ratio, as well as its Young's modulus values are similar to that of a natural human bone [15]. Magnesium has a greater fracture toughness compared to ceramic biomaterials such as hydroxyapatite [15]. Implants designed from biomaterials that have moduli which are not well matched with the modulus of natural human bone tissue may lead to poor recovery of the tissue or early fracture due to the effect known as stress-shielding [12]. Stress-shielding effects arise from shear stresses due to the difference in the material properties (also referred to as mechanical properties) of the implant and the human bone [16]. Stress shielding causes the stress to be concentrated at the tissue-implant interface, thus the recovery process of the

tissue may get slowed or even stunted because of the same stress shielding. However, with implants designed from biodegradable materials having mechanical properties like that of a natural bone e.g., magnesium, the issue of stress-shielding is addressed by transferring the load to the recovering tissue as the biodegradable material gradually degrades. The biodegradation (also referred to as corrosion) of magnesium in an aqueous environment is through electrochemical reactions. The same electrochemical reactions take place in the human body, provided the implant is engineered from magnesium.

When considering the use of magnesium as a temporary implant material, its fast corrosion rate poses significant challenges in various ways. During the corrosion process, the rapid biodegradation of magnesium releases large volumes of hydrogen gas, which can have detrimental effects on the surrounding tissue [17]. Additionally, the mechanical integrity of magnesium is compromised before the healing process is complete, which is problematic for most applications. To address these challenges, several approaches can be taken to control the corrosion rate of magnesium. One effective method is alloying, which involves incorporating other elements into the magnesium matrix. This technique not only reduces the degradation rate but also enhances the mechanical properties of the alloy. However, it is crucial to consider the biocompatibility of the alloying elements used, as some elements can have harmful effects on other organs within the body [18]. For instance, aluminium, while capable of slowing down the biodegradation rate of magnesium, is neurotoxic [19, 20]. Similarly, zinc exhibits high cytotoxicity and, at elevated levels, can cause genotoxicity [18]. Therefore, the selection of alloying elements must ensure that the biodegradation behaviour is improved without compromising the overall biocompatibility of the material.

There are two primary factors that contribute to the poor corrosion resistance of magnesium and its alloys. The first factor is the occurrence of micro-galvanic corrosion, which is triggered by the presence of second phases or inter-metallic impurities. This type of corrosion leads to accelerated degradation. The second factor is related to the protective film of hydroxide that forms on the surface of magnesium, known as the quasi-passive film. Unfortunately, this film is less stable compared to the

protective films found on other metals like stainless steel and aluminium. As a result, it fails to provide sufficient resistance against pitting, further exacerbating the corrosion issues experienced by magnesium and its alloys.

1.3. COMPUTATIONAL MODELLING

Computational modelling is a powerful and versatile approach that plays a crucial role in numerous scientific disciplines, ranging from engineering and physics to biology and chemistry. It basically involves the development and application of mathematical algorithms and computer simulations to understand complex systems, analyse data, and make predictions. By harnessing the computational power of modern technology, researchers are able to create virtual representations of real-world phenomena, allowing them to explore and manipulate variables in ways that may not be feasible with traditional experiments.

Computational modelling has simply revolutionised the field of engineering by enabling engineers to gain valuable insights into intricate processes, optimize designs, and solve intricate problems. It has become an indispensable tool that drives. Some of the widely used computational modelling tools (software) in the field of engineering include COMSOL Multiphysics, Abaqus, ANSYS, and MATLAB. These computational modelling tools are collectively known as Computer-Aided Engineering (CAE) software tools.

1.4. COMSOL MULTIPHYSICS

COMSOL Multiphysics, formerly known as FEMLAB, is a finite element analysis, solver and simulation software package for various physics and engineering applications. It can be used to model and simulate a wide range of physical phenomena like electrochemistry, structural mechanics, heat transfer, fluid flow and electromagnetics. COMSOL uses finite element techniques to solve complex partial differential equations (PDEs) of a given problem.

COMSOL Multiphysics provides a comprehensive platform for studying corrosion processes in various materials and environments. By incorporating detailed geometric parameters, material properties, and environmental conditions, engineers can analyse corrosion scenarios such as localised corrosion, galvanic coupling, species concentration, and corrosion under different coatings. The simulations performed in COMSOL aid in understanding corrosion mechanisms, optimising the selection of materials and designing effective corrosion protection strategies.

Some of the previous works to model and analyse corrosion using COMSOL Multiphysics include the simulation of galvanic corrosion of a mild steel bolt in a magnesium alloy (AZ91D) plate (Olanipekun et al.,2014) [21]. One of the dangerous types of corrosion known as pitting corrosion, was modelled and simulated by Al-Shemmary et al. (2021) [22]. Gupta et al. (2022) [23] performed a time-dependent analysis of galvanic corrosion on mild steel having a magnesium alloy (AE44) rivet-plate joint system using COMSOL Multiphysics simulation. Cui et al. (2023) [24] presented a new theoretical phase field-based formulation for predicting electro-chemo-mechanical corrosion in metals with COMSOL implementation.

Two different COMSOL Multiphysics modules known as the Electrochemistry module (The Primary and Secondary Current Distribution Interfaces) [25] and the Chemical Reaction Engineering module (The Nernst-Planck Equations Interface) [26] are used in this study to obtain the electrolyte potential and electrolyte current density magnitude plots, Tafel plots and the species concentration distribution profiles.

1.5. SCOPE OF THE THESIS

The entire objective of this work is to compare the three AT31 magnesium alloys regarding their corrosion resistance in a physiological corrosive environment as well as evaluate the effectiveness of the simulation methods for verifying the experimental findings related to their corrosion performance. The physiological environment considered in this study is the 0.9% Isotonic Sodium Chloride Solution (0.9% NaCl) also referred to as Isotonic Saline Solution having a pH of 5.6 [27, 28].

A comparison of the electrochemical parameters obtained from the experimental potentiodynamic polarisation curves and the simulated potentiodynamic polarisation curves is done. The simulated concentration profiles of the various electrochemical species of the three magnesium alloys are also compared.

PART 2

LITERATURE REVIEW

2.1. MAGNESIUM AS A BIODEGRADABLE MATERIAL

In the early 1850s, small amounts of magnesium were manufactured in the United States and Europe primarily for use in pyrotechnics and as igniting bands or wires for the emerging field of photography [29]. These early magnesium products were showcased at the 1862 world exhibition in London. The physician Edward C. Huse used some of the initial magnesium products presented at the 1862 world exhibition in London, specifically magnesium wires, as ligatures to stop the bleeding vessels of three human patients in 1878 [17]. Earlier studies also suggested the use of magnesium and its alloys in various medical applications [17, 29]. For many years magnesium attracted special interest in

Theoretically, an ideal biodegradable material for orthopaedic applications should possess performance characteristics that are in alignment with the reconstruction and recovery process of injured tissues. It should provide temporary mechanical support while gradually dissolving within the human body at an appropriate rate [30]. As the degradation progresses, the implant's mechanical integrity is expected to decline, as depicted in Figure 2.1. According to research, the bone healing process generally occurs in three stages: inflammation, repair, and remodelling [30]. In the initial inflammation stage, which lasts from 1 to 7 days, the immune system reacts to the presence of the implant as a foreign body. During the repair stage, tissue regeneration takes place, and the implant integrates with new bone tissue over a period of 3-4 months, depending on the type and location of the fracture. Finally, the remodelling stage, which is considered to be the longest stage of bone healing, involves the replacement of woven bone with cortical bone through regeneration and remodelling. This stage can take several months to years to complete. Over the years, magnesium

has attracted special interest as a biodegradable material for use in various implant applications, particularly temporary implant applications such as bone screws and bone plates in orthopaedic, and stents in cardiovascular implantology. However, the high corrosion rates of magnesium have posed challenges since its initial use in orthopaedics and other fields.

The high corrosion rates of magnesium simply imply swift corrosion. The swift corrosion does not provide enough time for tissue growth and full recovery before the implant prematurely degrades and fails. One of the influencing factors of the corrosion rate of magnesium is the corrosive nature of the surrounding environment, particularly in an environment containing chloride ionic species (Cl^-) such as human body fluids [31]. Literature shows that the swift degradation of magnesium may lead to the production of a significant amount of hydrogen gas, which can be detrimental to the body and needs to be avoided [12, 32]. Despite these challenges, magnesium is still of great interest due to its advantageous biodegradability and biocompatibility. Therefore, it is crucial to maintain appropriate corrosion rates for biodegradable magnesium implants.

Over the years, various alloying techniques such as incorporating aluminum, calcium, zinc, or silver, have been explored to enhance the corrosion resistance of magnesium. Aluminium (Al) and zinc (Zn) have shown promising results when it comes to increasing the corrosion resistance of magnesium [18, 30]. However, additional information is necessary to evaluate the biocompatibility of alloyed magnesium in the human body [18, 19]. Surface treatment techniques, including electroplating, electroless plating, conversion surface treatments, and anodization, can also help reduce corrosion. However, it is important to note that these coatings may lead to localized corrosion if there are any defects present.

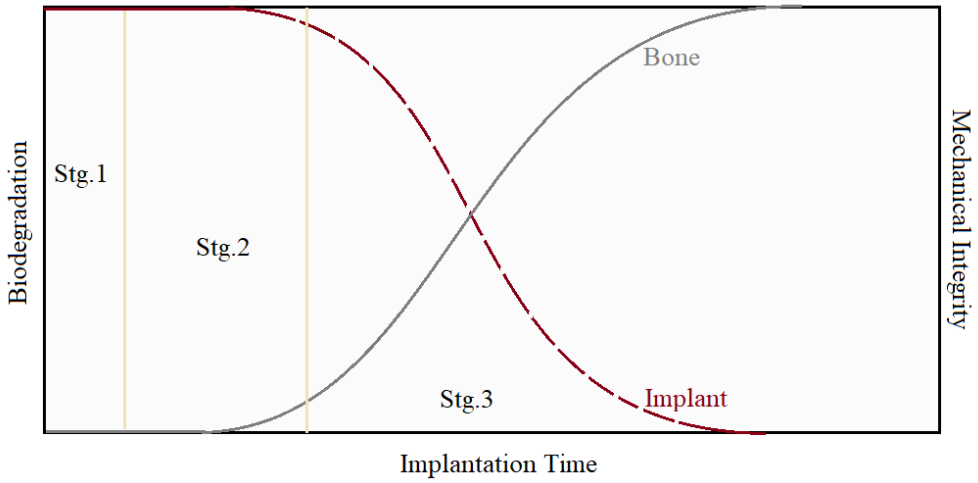

Figure 2.1. Schematic illustration of the biodegradation and mechanical integrity of an ideal implant during bone healing [30].

Stg.1 = Inflammation: hematoma formation with a typical inflammatory response lasting 1-7 days.

Stg.2 = Repair: hematoma → granulation tissue → connective tissue → cartilage → mineralization → woven bone; continues 4-6 months depending on the fracture position and type.

Stg.3 = Remodelling: woven bone is replaced by cortical bone and a medullary cavity is restored, which persists for several years.

2.2. BIOCOMPATIBILITY AND MECHANICAL PROPERTIES OF MAGNESIUM

2.2.1. Magnesium Biocompatibility

The biosafety and biocompatibility of absorbable biomaterials should be carefully considered since the material will enter the human body [33]. Therefore, the biocompatibility of a material is a crucial factor for successful implantation. According to the literature, biocompatibility is commonly defined as the ability of a material to interact favourably with living tissues in the human body without causing toxicity or immunological rejection. In the case of metallic biomaterials, biocompatibility is often

influenced by biocorrosion processes (or simply corrosion or degradation processes) within the human body. Corrosion of these materials may lead to the release of toxic metal ions like aluminium, zinc, nickel, chromium, and cobalt, which can trigger undesirable immune responses and tissue reactions such as inflammation and irritation. Exceeding the concentration limits of certain ions (e.g., zinc, aluminium, chromium, cobalt, and nickel) in the surrounding tissues or body fluids can result in detrimental tissue reactions. For instance, aluminium can cause muscle fibre damage and lead to the generation of Alzheimer's disease [33], and zinc is known to be neurotoxic and hinder bone development [33, 34], see Table 2.2. Consequently, these metallic implants do not possess optimal biocompatibility.

Magnesium stands apart from other metallic biomaterials due to its excellent biocompatibility. Interestingly, magnesium is the fourth most abundant inorganic element found in the human body. An average adult human body weighing around 70 kg contains approximately 24.31 g of magnesium [14, 18], with 50-60 percent of this amount stored in the skeletal system. To maintain appropriate magnesium levels, individuals need a daily allowance of 0.7 g of magnesium [18,34]. Moreover, magnesium plays an essential role in human metabolic functions, as mentioned in section 1.2 of chapter 2. Several studies have highlighted the critical role of divalent cations, including Mg^{2+}, in bone tissue remodelling and formation [35]. Additionally, magnesium is vital for the formation of hydroxyapatite, the biological mineral phase, on the surface of implanted devices. Other studies demonstrated that magnesium-based substrates promote bone cell attachment on the surface implant [36]. Furthermore, the presence of magnesium in orthopaedic implants has been shown to enhance the adhesion of osteoblastic cells and promote optimal osteogenesis.

2.2.1.1. Alloying

There are many various techniques used to improve the performance of magnesium including alloying. The mixing or combining of two or more metals together is what is referred to as alloying. It plays a fundamental role in improving the biodegradation and mechanical properties of magnesium. The mixture of magnesium and any other metallic element results in a magnesium alloy (Mg alloy). Magnesium alloys are of

particular interest in comparison to pure magnesium because of their improved resistance to corrosion and mechanical properties. Numerous metallic elements can be used as alloying elements for magnesium; however, it is essential to select appropriate elements that improve both the corrosion resistance and mechanical properties of magnesium while being non-toxic to assure the biocompatibility of the implant. Some of the properties and effects of the alloying elements used in biodegradable magnesium are outlined in Table 2.1 and Table 2.2 [18, 33, 34, 37, 38].

Table 2.1. A summary of the properties of some alloying elements.

Element	**Quantity in Human Being**	**Quantity in Human Bone**	**Blood Serum Level**	**Quantity in Blood**	**Daily Allowance**
Magnesium – Mg	25 g	1.7 mg/g	0.73-1.06 mM	900 µmol/L	0.7g
Calcium – Ca	1100 g	353.3 mg/g	0.919-0.993 mM	1300 µmol/L	0.8 g
Zinc – Zn	2 g	67 mg/Kg	12.4-17.4 µM	6.42 mg/L	15 mg
Manganese – Mn	12 mg	Nil	< 0.8 µg/L	5.67 µg/L	4 mg
Iron – Fe	4-5 g	91 mg/Kg	5.0-17.6 g/L	45-50 mg/cm^3	10-20 mg
Silicon – Si	1-2 g	Nil	9.5 µmol/L	< 44 µg/g	< 204 mg
Strontium – Sr	0.3 g	0.287 mg/g	0.17 mg	3 µmol/L	2 mg
Zirconium – Zr	< 250 mg	Nil	Nil	Nil	3.5 mg
Lithium – Li	Nil	Nil	2-4 ng/g	0.004 µmol/L	Nil
Yttrium – Y	Nil	Nil	< 4.7 µg	Nil	Nil
Rare Earth Element – REE's	Nil	Nil	Nil	Nil	Nil

Table 2.2. A summary of the effects of some alloying elements in biodegradable Mg alloys.

Element	Role	Toxicology
Aluminium (Al)	Its presence leads to significant grain refinement. The addition of smaller quantities of Al of about 1-5% ends up in an equiaxed grain transition and substantial grain size reduction. Larger quantities (>5%) on the other hand do not affect the grain size. The presence of aluminum enhances the corrosion resistance.	Neurotoxic in higher concentration and accumulation in bone; Risk factor in generation of Alzheimer's disease; Can cause muscle fiber damage.
Zinc (Zn)	Over 85% of the zinc content is found in the muscular and skeletal systems. It enhances the strength required to withstand pressure, diminishes the release of hydrogen gas in biocorrosion processes, and counteracts the detrimental corrosive impact of iron and nickel contaminants that may be present in the magnesium alloy.	Neurotoxic and hinder bone development at higher concentration.
Calcium (Ca)	The skeletal framework of the human body predominantly holds approximately 99.5% of the overall calcium content. This presence of calcium contributes to enhancing resistance against corrosion and facilitating the process of grain refinement. Additionally, it plays a vital role in sustaining an appropriate level of bone density to effectively support the body's structural integrity.	Calcium metabolism disorder; kidney stones.
Manganese (Mn)	Manganese provides advantages for the maintenance of strong bone structure and the regulation of bone processes, contributing to the production of enzymes essential for bone development. Furthermore, it enhances the refinement of grains and enhances the tensile strength and resistance to corrosion of magnesium.	Neurotoxic in higher concentration (manganism)
Tin (Sn)	Tin has the capacity to stimulate the synthesis of proteins and nucleic acids, which are crucial for the growth and development of the bone. It enhances the compressive strength of the bone and resistance against corrosion.	Excessive Sn results in stomachache, anemia, and liver and kidney problems.
Rare Earth Elementa (REE's)	Lanthanum (La), gadolinium (Gd), and neodymium (Nd) are examples (REEs). The inclusion of yttrium (Y) enhances the malleability of materials but diminishes their ability to resist corrosion and interact well with biological systems. On the other hand, neodymium (Nd) enhances the attachment of cells and improves biocompatibility. Lanthanum (La) and gadolinium (Gd) play a positive role in enhancing the resistance of magnesium alloys to corrosion.	Intake of REE over a long time would exert a harmful influence on the human liver and kidney and result in some negative effects on immunity.

2.2.2. Mechanical Properties of Magnesium

The mechanical properties of metallic biomaterials used in orthopaedic applications should be similar to that of a human bone (natural bone). The implantation of biomaterials, like bone plates, and screws, into the human body is to assist with the healing process of the damaged/diseased bone tissue by offering it support, therefore, the mechanical properties of the used biomaterial should match that of the tissue. However, most of the commonly used biomaterials (titanium alloys, stainless steel, and cobalt-chromium-based alloys) possess higher mechanical properties in comparison to that of the human bone. Such biomaterials may not be the most suitable choice for orthopaedic applications because of their higher mechanical properties. The mismatch in mechanical properties of the implant and the tissue can lead to poor recovery of the tissue because of the stress shielding effect [12, 16]. The stress shielding effect occurs when the normal stress on the bone is reduced after implantation, resulting in a decrease in bone tissue density. In a healthy individual, bone tissue adapts to external forces by remodelling itself. Hence, if the stiffness of the implant material differs significantly from that of natural bone tissue, the reduced loading on the bone can weaken it over time.

The mechanical properties of magnesium and its alloys are more similar to that of a human bone. This means that the stress shielding effects can be reduced with implants constructed from magnesium and its alloys. Table 2.3 compares the mechanical properties between various metallic biomaterials, magnesium and its alloys, and the human bone (cortical bone) [39].

Table 2.3. Summary of the metallic biomaterials and cortical bone comparison.

Mechanical Properties	**Cortical Bone**	**Pure Mg & its alloys (AZ31, AZ91, ZM21)**	**Stainless Steel (316L)**	**Ti-based alloys (Ti-6Al-4V, Ti-6Al-7Nb)**	**Co-based alloys (CoCr alloys)**
Density *(g/cm^3)*	1.8-2.0	1.74	7.9	4.4	7.8
Elastic Modulus *(GPa)*	5-23	41-45	190	110	210-253
Yield Strength *(MPa)*	104.9-114.3	130	221-1213	485	448-1606
Tensile Strength *(MPa)*	35-283	220	586-1351	760	655-1896

2.3. ELECTROCHEMISTRY OF MAGNESIUM

2.3.1. Definition

Electrochemistry is a science that studies chemical reactions which take place at the interface of an electron conductor (electrode) – usually a metal, and an ionic conductor (electrolyte). The chemical nature and structure of a metallic surface which is in contact with an electrolyte will undergo electrochemical reactions on its surface. These reactions explain corrosion science – how corrosion reactions occur. The corrosion process of metallic materials typically involves electrochemical reactions that produce hydrogen, oxides, and hydroxides.

In aqueous environments, the process of corrosion proceeds occurs through an electrochemical process in which two distinct locations on the interface of the metallic surface and the corrosive environment facilitate both anodic (oxidation) and cathodic (reduction) reactions. The former is characterised by the loss of electrons while the latter is characterised by the gain of electrons. These reactions occur as a result of the flow of electrons and ions between the electrode and the electrolyte.

2.3.2. Electrochemical Nature of Aqueous Corrosion

Aqueous corrosion, also known as wet corrosion, is an electrochemical process that occurs when a metal is exposed to a corrosive environment, typically a liquid medium. Aqueous corrosion involves the transfer of electrons or ions between distinct regions (or locations) on the surface of the metal. The corrosion mechanism can be classified by two main electrochemical reactions; oxidation reaction (also known as anodic reaction) and reduction reaction (also referred to as cathodic reaction). These reactions are collectively known as REDOX reactions. At the anodic region or simply anode, the metal loses electrons and undergoes oxidation and consequently the formation of metal ions. These metal ions then migrate through the liquid medium to the cathode or cathodic region. Reduction reactions occur at the cathode and metal ions combine with water or other species to form corrosion deposits or products. Over time, this continuous flow of electrons and migration of ionic species greatly contribute to the degradation of the metal.

In an aqueous environment, magnesium degradation proceeds by the electrochemical reaction shown below, equation 2.1 through equation 2.5. The degradation of magnesium is schematically shown in Figure 2.2 [40]. Magnesium materials are susceptible to both general and localised corrosion. The distinctive property of magnesium's electronegative potential increases the susceptibility of its alloys to galvanic corrosion. This type of corrosion can occur internally due to components within the microstructure that have lower active potential, such as second phases or impurities.

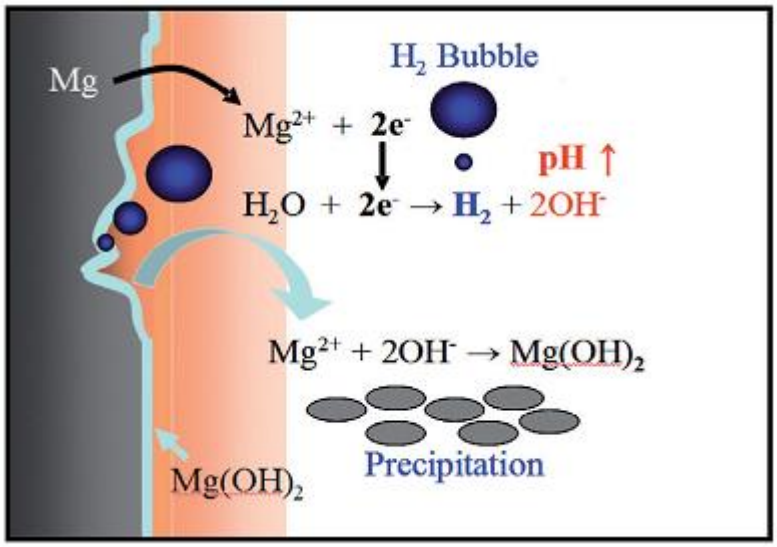

Figure 2.2. A schematic representation of the degradation of magnesium [40].

The electrochemical reactions of the corrosion of magnesium can be categorised into two, oxidation reaction and reduction reactions. The primary electrochemical reactions on the surface of magnesium are given by the equations below.

$$Mg_{(s)} \rightarrow Mg^{2+}_{(aq)} + 2e^- \quad (2.1)$$

$$2H^+_{(aq)} + 2e^- \rightarrow H_{2(g)} \quad (2.2)$$

$$2H_2O_{(l)} + 2e\text{-} \rightarrow H_{2(g)} + 2OH^-_{(aq)} \quad (2.3)$$

$$Mg_{(s)} + H^+_{(g)} + H_2O_{(l)} \rightarrow Mg^{2+}_{(aq)} + H_{2(g)} + OH^-_{(aq)} \quad (2.4)$$

$$Mg^{2+}_{(aq)} + 2OH^-_{(aq)} \rightarrow Mg(OH)_{2(s)} \quad (2.5)$$

Equation (2.1): half-cell anodic reaction of magnesium oxidation, at the anode.
Equation (2.2): half-cell cathodic reaction of hydrogen ion reduction, at the cathode.
Equation (2.3): water reduction reaction, at the cathode.
Equation (2.4): overall reaction of magnesium corrosion in an aqueous environment.
Equation (2.5): product formation reaction.

The equations above show that magnesium ions (Mg^{2+}) are generated at the anode and hydrogen gas (H_2) is produced at the cathode, respectively. The equations also show that there is a generation of hydroxide ions (OH^-) and a consumption of hydrogen ions (H^+).

A comparison of the reaction quotient (Q_{sp}) and the solubility product (K_{sp}), also known as the solubility product constant, is one way to predict whether a precipitate of a substance will form in a given solution. The reaction quotient (Q_{sp}) of equation (2.5) can be calculated using equation (2.6). Equation (2.5) shows the formation of magnesium hydroxide which has the chemical formula $Mg(OH)_2$, molecular weight of 58.3197 g/mol, and a solubility product of 5.61×10^{-12} [41]. When the reaction quotient is greater than the solubility product, a precipitate will form. This information holds significance as it enables us to compare the concentrations of different ions and determine whether magnesium hydroxide will precipitate or not.

$$Q_{sp} = [Mg^{2+}]\,[OH^-]^2 \tag{2.6}$$

PART 3

EXPERIMENTAL STUDIES

The upcoming sections in the chapter describe the composition of the Mg alloyed in this study and the experimental procedures that were performed.

3.1. MATERIALS

The magnesium alloy used in this study was AT31, which was produced by casting. Türkiye served as a primary supplier of pure magnesium (Mg), pure aluminium (Al), and pure tin (Sn), while the People's Republic of China provided the main alloys, and a custom-made die was used for the manufacturing process, low-pressure permanent mould (LPPM) casting was used, as shown in Figure 3.1 [42, 43]. In order to remove segregations after casting, the material (alloy) was homogenised at 350°C. Hot rolling was performed at three different temperatures, 350°C, 400°C, and 500°C, to deform the alloy from 5 mm to 3.5 mm, 4.0 mm, and 4.5 mm thicknesses, thus resulting in three different sample classifications (Mg350s, Mg400s, and Mg500s respectively). During hot rolling, the thickness deformation rates were 30%, 20%, and 10% respectively. Each sample class contained 9 samples, amounting to a total of 27 samples. After conducting the necessary experiments, only three samples were used in this study. The elemental composition of the AT31 alloy is summarized in Table 3.1

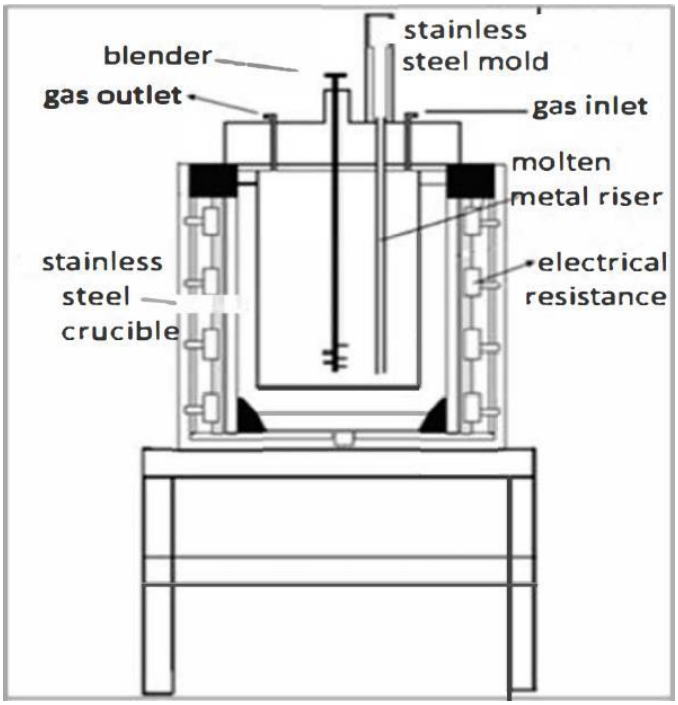

Figure 3.1. Low-pressure permanent mold (LPPM) casting [42, 43].

Table 3.1. Elemental composition of the AT31 alloy (weight %)

Elements	Al	Sn	Mn	La	Gd	Mg
wt%	2.50	1.00	0.30	0.40	1.33	Bal.

3.2. SAMPLE PREPARATION

3.2.1. Metallographic Grinding and Polishing

In the current work, a metallographic grinding and polishing machine was used to successfully perform the grinding and polishing processes, as can be seen in Figure 3.2. Each sample was accurately ground and then polished.

Metallographic grinding removes damaged or deformed surface layers from a metal sample through abrasive grinding while introducing as little new deformation as possible. In this study, coarse-grit silicon carbide papers were used to remove any surface imperfections. This process was performed with the use of finer-grit silicon carbide papers progressively. 800-grit and 1200-grit silicon carbide papers are some

of the papers that were used. This step is crucial to ensure that the subsequent polishing stage produces accurate and reliable results.

Metallographic polishing was the next step right after grinding. This process aims to create a smooth and reflective surface on the metal surface. One polishing pad was used to polish the different samples used in this study. This stage removes the damage caused by grinding and produces a mirror-like surface finish for better observation of the microstructure as well as a well-finished metal for properly conducting the potentiodynamic polarisation test.

Figure 3.2. Metallographic grinding and polishing machine.

3.2.2. Cold Mounting

Cold mounting, also referred to as cold embedding or castable mounting, is a method used to encapsulate metallographic samples in a resin material without the need for pressure or heat. This process typically involves mixing a two-part epoxy resin, part A – Resin and part B – curing agent. The mixture of the two components together prompts a chemical reaction between part A and part B, transforming them from a liquid mixture into a solid over time.

The samples were each placed into a square plastic mould (ice cube tray) together with an insulated copper wire attached to individual samples and the two-epoxy resin mixture was poured into them. The epoxy resin was left to cure at room temperature

for 24 hours, creating a solid transparent mount that securely holds the sample in place. After removing the samples from the mould, they were ground and polished in readiness for a potentiodynamic polarisation test. The exposed surfaces of the samples were covered with perforated insulation tape, only leaving 19.63 mm^2 of surface area exposure in each sample as can be seen in Figure 3.3.

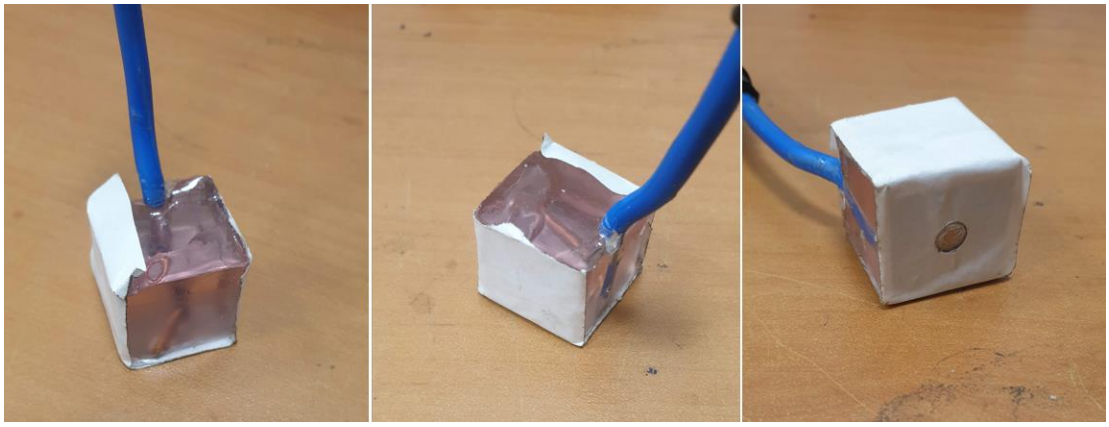

Figure 3.3. Magnesium sample embedded in epoxy with only 19.63 mm2 surface area exposure.

3.3. ELECTROLYTE SOLUTION

The electrolyte solution is one of the fundamental elements of a corrosion cell. An electrolyte solution serves as a conductive medium through which ionic species can move, thereby enabling electrochemical reactions to take place. The conductivity of an electrolyte is an important factor as it is the measure of an electrolyte solution to conduct electrical current. A higher electrolyte conductivity simply indicates a greater ability of the electrolyte to transport ionic species and facilitate the process of corrosion. The electrolyte solution used in this study is 0.9% NaCl (0.9% Isotonic Sodium Chloride Solution). According to the literature, the conductivity value of 0.9% NaCl is 16 mS/cm at 25°C.

Figure 3.4. 0.9% Isotonic Sodium Chloride Solution (0.9% NaCl).

3.4. ELECTROCHEMICAL MEASUREMENTS

3.4.1. Potentiodynamic Polarisation Test

The potentiodynamic polarisation test, also known as the DC polarisation test, is an electrochemical technique widely used to investigate the corrosion behaviour of metallic materials in various corrosive environments. DC polarisation test provides valuable information about the electrochemical reactions taking place at the metallic material's surface. With the provided information from the test, an evaluation of the corrosion resistance of a metallic material can be performed.

In this study, the biocorrosion of the magnesium samples was evaluated by the DC polarisation test using a three-electrode cell – a *working electrode*, a *reference electrode*, and a *counter electrode* [44], as shown in Figure 3.5 (a). 0.9% Isotonic Sodium Chloride Solution, 0.9% NaCl, at 37 °C was used as an electrolyte.

Working electrode: this is a primary electrode under investigation. It is the electrode where the electrochemical reactions occur. The term working electrode is used instead of anode because the investigations are not limited to the electrode's anodic behaviour alone, its cathodic behaviour can also be investigated. The working electrodes used in this experimental procedure were the magnesium samples (Mg350s, Mg400s, and Mg500s)

Reference electrode: this is used as a reference point for measuring the potential of the working electrode. It maintains a stable datum against which the potential of the working electrode can be measured. Typically, the electrochemical potential of a reference electrode remains the same if there is no current passing through it. The most used reference electrodes include the saturated calomel electrode (SCE) and the silver/silver chloride (Ag/AgCl) electrode.

Counter electrode: also known as an auxiliary electrode, a counter electrode is a conductor that completes an electrochemical cell circuit. It creates a path for the current to flow, meaning that the current that flows into the solution through the working electrode leaves the solution through the counter electrode, thus allowing the electrochemical reactions to take place at the working electrode. Generally, an inert conductor such as platinum or graphite can be used as counter electrodes. A counter electrode made of graphite was used in this experimental procedure.

The samples were polished before dipping them into 0.9% NaCl solution. A fixed opening of 19.63 mm^2 was made on the insulation tapes taped on the sample surface to expose this surface to the solution, see Figure 3.3. This exposed surface area functioned as the working electrode. The potentiodynamic polarisation test yields polarisation curves (discussed in Chapter 5). The GAMRY software was used to fit these curves and determine the corrosion current and the corrosion potential values for various samples as shown in Figure 3.5 (b).

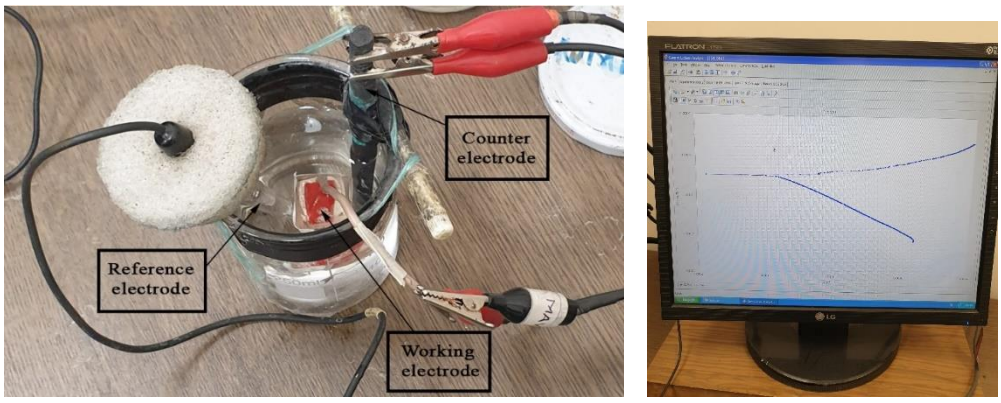

(a) (b)

Figure 3.5. Experimental set-up used for a three-electrode electrochemical cell test in 0.9% NaCl (a). Polarisation curve in GAMRY software (b).

3.4.2. Corrosion Rate Calculation

The corrosion rate in terms of penetration rate (CR) can be calculated by Faraday's Law. The corrosion rate (rate of penetration) calculations performed in this study are done by using the ASTM Standard G102-89 [45]. The corrosion rate (CR) according to ASTM Standards is given as:

$$CR = K_1 \frac{i_{corr}}{\rho} EW \tag{3.1}$$

CR = corrosion rate (mm/yr.).
K_1 = constant, 3.27×10^{-3} (mm g/μA cm yr.).
i_{corr} = corrosion current density (μA/cm^2).
ρ = density (g/cm^3).
EW = equivalent weight.

The equivalent weight, EW, is given as:

$$EW = \frac{1}{\sum \frac{n_i f_i}{W_i}} \tag{3.2}$$

W_i = the atomic weight of the i^{th} element in the alloy.
n_i = the valence of the i^{th} element in the alloy.
f_i = the mass fraction of the i^{th} element in the alloy.

Generally, when using equation 3.2, only elements above 1 mass percent in the alloy are included in the calculation. Table 3.2 shows the values of the parameters used to calculate the equivalent weight of AT31 alloy. The density is 1.738 g/cm^3, and the equivalent weight (EW) of the alloy was calculated to be 12.242.

Table 3.2. Parameters used to calculate equivalent weight of AT31 alloy.

Element	Atomic Weight – W_i	Mass Fraction – f_i	Valence – n_i
Mg	24.305	95.17	2
Al	26.982	2.50	3
Gd	157.250	1.33	3
Sn	118.710	1.00	4

3.5. IMMERSION CORROSION TEST

Immersion corrosion, also referred to as the weight loss technique, is a widely used technique to assess the corrosion behaviour of a material in each corrosive environment. It provides a simple and practical way of evaluating the corrosion resistance of materials. The measurement of the weight loss of a material gives insight into its susceptibility to corrosion.

After the potentiodynamic polarisation test of the 27 AT31 alloy samples, 3 samples were chosen (Mg353, Mg403, and Mg503) and prepared for the immersion test. The 3 samples of the AT31 alloys were cut into sections ($10\ \text{mm} \times 10\text{mm} \times 3\text{mm}$) and polished with a polishing pad. After polishing, the samples were cleaned with distilled water and ethanol, and then air dried. The initial weight and surface area of the samples were measured before the test. The test was carried out in 0.9% NaCl solution at a constant temperature of 37 °C. The samples were wrapped in plastic nets and placed into the 0.9% NaCl solution as shown in Figure 3.6 (a-c). They were taken out after a period of time (on the fourth day) then cleaned with distilled water and air dried and weighed immediately with a weighing balance machine, see Figure 3.6 (d). After weighing, the samples were wrapped into plastic nets and placed back into the solution. The weight changes were measured and recorded for each sample and discussed in Chapter 5.

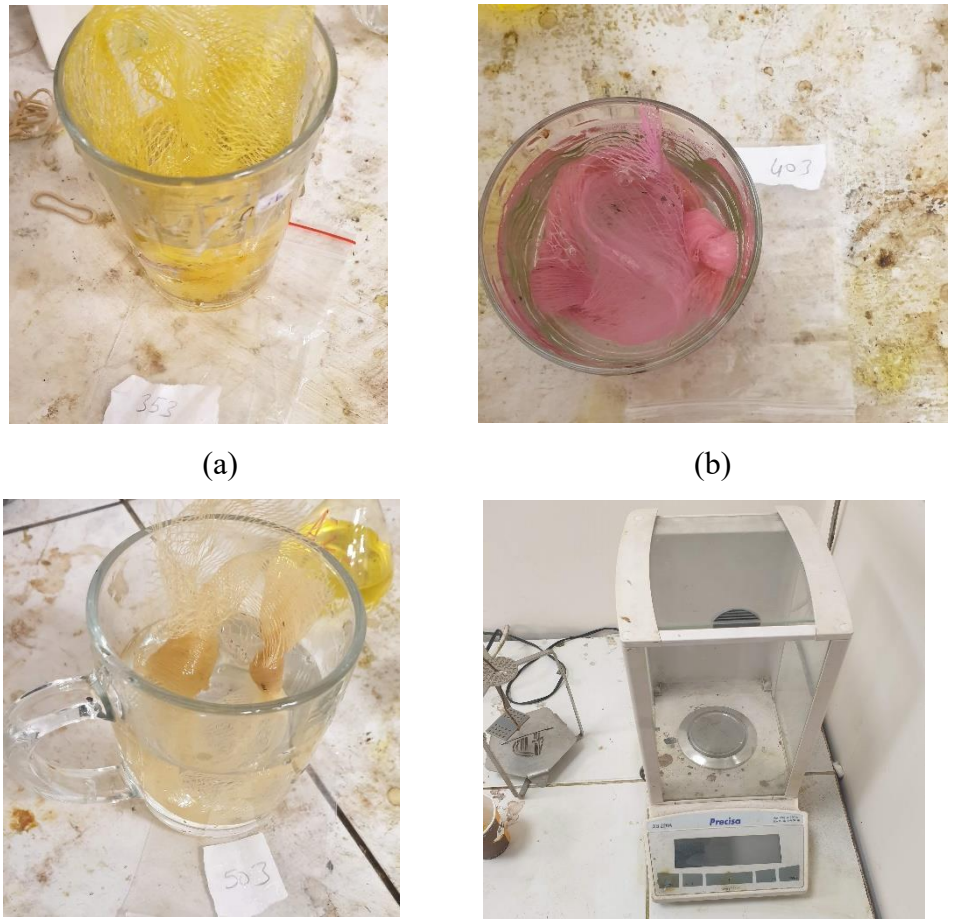

(a) (b)

(c) (d)

Figure 3.6. Mg353 immersed in 0.9% NaCl (a). Mg403 immersed in 0.9% NaCl (b). Mg503 immersed in 0.9% NaCl (c). Weighing balance machine (d).

PART 4

MODELLING METHODOLOGY

The physics of mass transportation, governing equations and assumptions, geometry modelling, domain conditions, and boundary conditions used in this study are described in detail in this chapter.

4.1. MASS TRANSPORT

Mass transport is a fundamental concept in most fields of engineering. From a physics, chemistry or chemical engineering perspective, mass transport is an electrolysis reaction that refers to the movement of ions (anions or cations) or molecules between an electrode surface and the electrolyte solution. Typically, there are three different mechanisms of mass transport that can influence an electrolysis reaction. These mechanisms include diffusion, convection, and migration.

4.1.1. Diffusion Mechanism

Diffusion is a fundamental mechanism that describes the natural tendency of species (ions, molecules, or particles) to distribute themselves evenly. In an electrolysis cell, there is a concentration gradient between the electrode surface and the bulk of the electrolyte solution due to the presence of positively and negatively charged ions. This concentration gradient drives the diffusion of species towards or away from the electrode surface. Diffusion can then be defined as the movement of species from a region of higher concentration to a region of lower concentration, resulting in concentration equalisation throughout the medium (e.g., electrolyte solution) over time.

The rate of movement of species by diffusion can be evaluated mathematically with Fick's law (named after a German physiologist, *Adolf Eugen Fick*). According to *Fick's law of diffusion*, the diffusion flux is proportional to the diffusion coefficient and the concentration gradient. The flux due to diffusion is given by equation (4.1). The negative sign indicates the movement of the species down a concentration gradient, from regions of higher concentrations to those of lower concentration.

$$N_{diffuion} = -D_i \nabla c_i \quad (4.1)$$

$N_{diffusion}$ = the rate of species by diffusion.
D_i = the diffusion coefficient of the species *i*.
c_i = the concentration of the species *i*.

Diffusivity, also referred to as diffusion coefficient, is a measure of how fast a concentration becomes uniform throughout medium over time. It is a constant of proportionality between the diffusion flux and the concentration gradient. The diffusion coefficients of various ions used in this study are presented in Table 4.1 [46, 47].

Table 4.1. Diffusivities of ions in an electrolyte solution at 25 °C (298.15 K) [46, 47].

Species	**Diffusivity *(m^2/s)***
Mg^{+2}	7.063×10^{-10}
H^+	9.312×10^{-9}
OH^-	5.273×10^{-9}
Na^+	1.334×10^{-9}
Cl^-	2.032×10^{-9}

4.1.2. Convection Mechanism

Convection is a mass transport mechanism that refers to the movement of mass through a fluid medium due to the differences in temperature or density within the fluid. When a fluid is heated, it causes the species in the fluid to gain energy and become less dense resulting in the rising of the species of the heated fluid while the cooler denser fluid in

the surrounding regions sinks. This creates a pattern referred to as a convection current. Convection currents can carry ions along with them.

There are two forms of convection, natural convection (a form of convection that typically relies on inherent properties of a fluid such as density and temperature gradients to generate the movement of ions) and forced convection (a form of convection that is involved with the application of an external force to induce and control the movement of ions in a fluid). Convection can also be classified based on flow regimes, laminar or turbulent flow. The former is characterised by a smooth and stable fluid flow with well-defined streamlines, while the latter is characterised by an irregular and chaotic fluid flow with no well-defined streamlines. Thus, the flux density due to convection is given as:

$$N_{convection} = c_i u \tag{4.2}$$

$N_{convection}$ = the flux density due to convection.
c_i = the concentration of the species *i*.
u = the bulk velocity vector of the solution.

4.1.3. Migration Mechanism

Migration, also referred to as electromigration, is a mass transport mechanism that refers to the movement of charged species in an electrolyte solution under the influence of an electric field. Electromigration is a crucial mechanism in various electrochemical processes such as corrosion and electrolysis.

When an electrolyte solution is subjected to an electric field via an electrode surface, positive ions (cations) from positive potential migrate to a negative electrode (cathode), while negative ions (anions) from negative potential migrate to a positive electrode (anode) along the direction of an electric field. This migration of charged species (ions) is known as electromigration, or simply migration. Thus, the flux due to electromigration is given as:

$$N_{migration} = -z_i u_{m,i} F c_i \nabla V \quad (4.3)$$

$N_{migration}$ = the flux due to electromigration.

z_i = the charge number of the ionic species *i*.

$u_{m,i}$ = the ionic mobility of the species *i*.

F = Faraday's constant.

c_i = the concentration of the species *i*.

V = the electric potential.

The ionic mobility of the species *i* in a solution can be calculated using the equation (4.4).

$$u_{m,i} = \frac{D_i}{RT} \quad (4.4)$$

D_i = the diffusion coefficient of the species *i*.

R = Universal gas constant.

T = Temperature.

The ionic mobilities of the species in this study are shown in Table 4.2.

Table 4.2. Ionic mobilities in an electrolyte solution at 25 °C (298.15 K).

Species	**Ionic Mobility *(s·mol/kg)***
Mg^{+2}	2.8493×10^{-13}
H^{+}	3.7566×10^{-12}
OH^{-}	2.1272×10^{-12}
Na^{+}	5.3816×10^{-13}
Cl^{-}	8.1975×10^{-13}

4.2. GOVERNING EQUATION

The total flux due to mass transport by diffusion mechanism, electromigration mechanism and convection mechanism is given by the Nernst-Planck Equation,

equation (4.5) [26]. The Nernst-Planck equation describes the movement of charged species within an electrolyte solution.

$$\mathbf{N}_i = -D_i \nabla c_i - z_i u_{m,i} F c_i \nabla V + c_i \boldsymbol{u} \tag{4.5}$$

Where $\mathbf{N}_i$ (vector) is the flux of the ionic species *i* [mol/(m^2·s)], D_i is the diffusion coefficient of the species *i* [m^2/s], c_i is the concentration of the species *i* [mol/m3], z_i is the charge number of the ionic species (dimensionless), $u_{m,i}$ ionic mobility of the species *i* [s·mol/kg], F refers to the Faraday's constant [s·A/mol], V denotes the electric potential (can also be written as Φ_l (scalar) – electrolyte potential [25]) [V], and $\boldsymbol{u}$ is the solvent velocity [m/s].

4.3. ASSUMPTIONS, GEOMETRY, AND BOUNDARY CONDITIONS FOR SECONDARY CURRENT DISTRIBUTION INTERFACE

The Secondary Current Distribution accounts for the current pathways that exist between two electrode surfaces within a conducting medium. It is used to compute current density distribution, potential distribution, and other related parameters. The current flow in an electrolyte is given as:

$$\mathbf{i}_l = F \sum z_i \mathbf{N}_i \tag{4.6}$$

Substituting $\mathbf{N}_i$ into equation (4.6) we obtain equation (4.7). Equation (4.7) is applicable to the *Tertiary Current Distribution Interface*.

$$\mathbf{i}_l = -F \sum D_i z_i \nabla c_i - \frac{F^2}{RT} \nabla \Phi_l \sum z_i^2 D_i c_i + \boldsymbol{u} \sum z_i c_i \tag{4.7}$$

4.3.1. Assumptions Involved in This Interface for The Current Study

- Two-dimensional geometry.
- The electrolyte solution is stationary.
- Oxidation and reduction reactions take place on the electrode surface.

- Initial electrolyte potential is taken as zero.
- Thoroughly mixed electrolyte solution, thus negligible concentration gradient.
- A stationary study is used to solve the problem.

The current flow in the electrolyte will be based on migration. Therefore, the current flow is given as:

$$\mathbf{i}_l = -\frac{F^2}{RT}\nabla\Phi_l \sum z_i^2 D_i c_i \tag{4.8}$$

The electrolyte conductivity can be obtained from equation (4.8) and is given as:

$$\sigma_l = -\frac{F^2}{RT}\sum z_i^2 D_i c_i \tag{4.9}$$

Equation (4.8) can be written as shown below in equation (4.10). Equation (4.10) is used in the *Secondary Current Distribution* interface.

$$\mathbf{i}_l = -\sigma_l \nabla\Phi_l \tag{4.10}$$

Overall, secondary current distribution aids with the understanding of local variations in current density and potential in electrochemical systems. It is, for this reason, it is used in this study to obtain the electrolyte potential and electrolyte current density plots, as well as the potentiodynamic polarisation curves.

4.3.2. Geometry and Boundary Conditions

For corrosion analysis, a half-cell reaction model with a single electrolyte domain is configured in COMSOL Multiphysics. The 2D geometry consists of an electrolyte domain with a width of 5mm, a working electrode at the extreme left edge with a height of 5mm, and a counter electrode at the extreme right edge with a height of 5mm. Table 4.3 contains the input parameters used in this simulation. The redox reactions take place on the working electrode. A triangular extra fine mesh is used for meshing. The Butler-Volmer equation, equation (4.11), is used to describe the electrode kinetics on

the working electrode and the initial electrolyte potential on the counter electrode is set to zero. Insulation boundary conditions are applied to all other boundaries of the electrolyte domain. Figure 4.1 shows a 2D meshed geometry used for all three distinct simulations of the three samples in this interface. Table 4.4 shows the description of the boundary conditions.

$$\boldsymbol{i}_{net} = i_{corr}\left\{exp\left(\frac{\alpha_a F\eta}{RT}\right) - exp\left(\frac{-\alpha_c F\eta}{RT}\right)\right\} \tag{4.11}$$

The electrolyte potential used for configuring the half-cell reaction model is taken as zero.

$$\boldsymbol{\Phi}_{l,bnd} = 0 \tag{4.12}$$

The insulation boundary condition defines the boundaries of a cell where electric current does not occur and is given as:

$$-\mathbf{n} \cdot \mathbf{i}_l = 0 \tag{4.13}$$

$\mathbf{i}_l$ = electrolyte current density.
σ_l = the electrolyte conductivity.
$\boldsymbol{i}_{net}$ = the net current density.
i_{corr} = the corrosion current density.
α_a = the anodic transfer coefficient.
α_c = the cathodic transfer coefficient.
η = the overpotential.
$\boldsymbol{\Phi}_{l,bnd}$ = the anodic transfer coefficient.
α_a = the anodic transfer coefficient.
α_a = the anodic transfer coefficient.
$\mathbf{n}$ = normal vector.

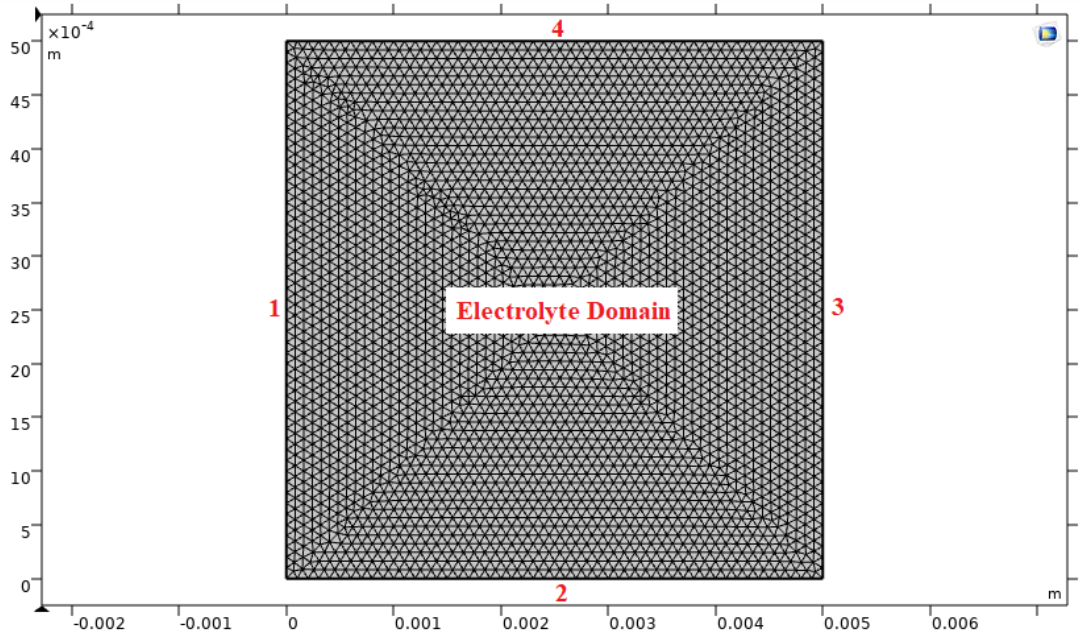

Figure 4.1. Schematic 2D meshed geometry in COMSOL Multiphysics.

Table 4.3. Parameter table.

Name	Value	Description
sigma	16mS/cm	Electrolyte conductivity
Temp	298.15K	Temperature
L1	5mm	Electrolyte domain thickness
L2	5mm	Working electrode height
L3	5mm	Counter electrode height
i_corr (Mg353)	2.4866e-5A/cm^2	Corrosion current
E_corr (Mg353)	-1.2940V	Corrosion potential
i_corr (Mg403)	1.3564e-5A/cm^2	Corrosion current
E_corr (Mg403)	-1.2769V	Corrosion potential
i_corr (Mg503)	6.066e-6A/cm^2	Corrosion current
E_corr (Mg503)	-1.224V	Corrosion potential

Table 4.4. Boundary conditions for geometry in Figure 4.1.

Boundary	Boundary Conditions
1	Electrode Surface
2	Insulation
3	Electrolyte Potential
4	Insulation

4.4. ASSUMPTIONS, GEOMETRY, AND BOUNDARY CONDITIONS FOR NERNST-PLANCK EQUATIONS INTERFACE

The Nernst-Planck Equations interface is used to model the transport of chemical species, including charged species (ions), in a conductive medium under the influence of concentration gradients and electric fields. The version of the Nernst-Planck equation shown below treats transport by convection, diffusion, and migration of individual dissolved species [26].

$$\frac{\partial c_i}{\partial t} + \nabla \cdot (c_i \boldsymbol{u}) = -\nabla \cdot \left(-D_i \nabla c_i - u_{m,i} F c_i \nabla V\right) + R_i = -\nabla \cdot \mathbf{J}_i + R_i \tag{4.14}$$

R_i = the reaction term.
$\mathbf{J}_i$ = the molar flux relative to convective transport.

4.4.1. Assumptions Involved in This Interface for The Current Study

- Two-dimensional geometry.
- The electrolyte solution is stationary ($\boldsymbol{u} = 0$).
- A steady-state condition $\left(\frac{\partial c_i}{\partial t} = 0\right)$.
- Oxidation and reduction reactions take place on the electrode surface.
- Only general corrosion occurs, thus galvanic corrosion is neglected.
- Thoroughly mixed electrolyte solution, thus negligible reaction term (R_i).
- Symmetric geometry about Y-axis. Half of the actual geometry is modelled.
- A stationary study is used to solve the problem.

Apart from transport equations, the physics interface assumes that the electroneutrality condition holds, this simply implies that the net charge in every control volume is zero [26].

$$\sum z_i c_i = 0 \tag{4.15}$$

With the above assumptions, equation (4.14) is reduced to the equation below which is used in the current model.

$$-D_i\nabla^2 c_i - z_i u_{m,i} F\nabla \cdot (c_i \nabla V) = 0 \qquad (4.16)$$

4.4.2. Geometry and Boundary Conditions

For corrosion analysis, a 2D geometry is modelled with a single electrolyte domain in COMSOL Multiphysics. The 2D geometry consists of an electrolyte domain with a width of 5mm and height of 5mm, a working electrode (magnesium surface) at the bottom left edge with a length of 2.5mm, and insulation tape at the bottom right edge with a length of 2.5mm. Table 4.5 contains some of the input parameters used in this simulation. The redox reactions take place on the working electrode. A triangular extra fine mesh is used for meshing, with additional smaller size settings for increased resolution on the magnesium electrode surface. Figure 4.2 shows a 2D meshed geometry used for all the distinct simulations of the three samples in this interface.

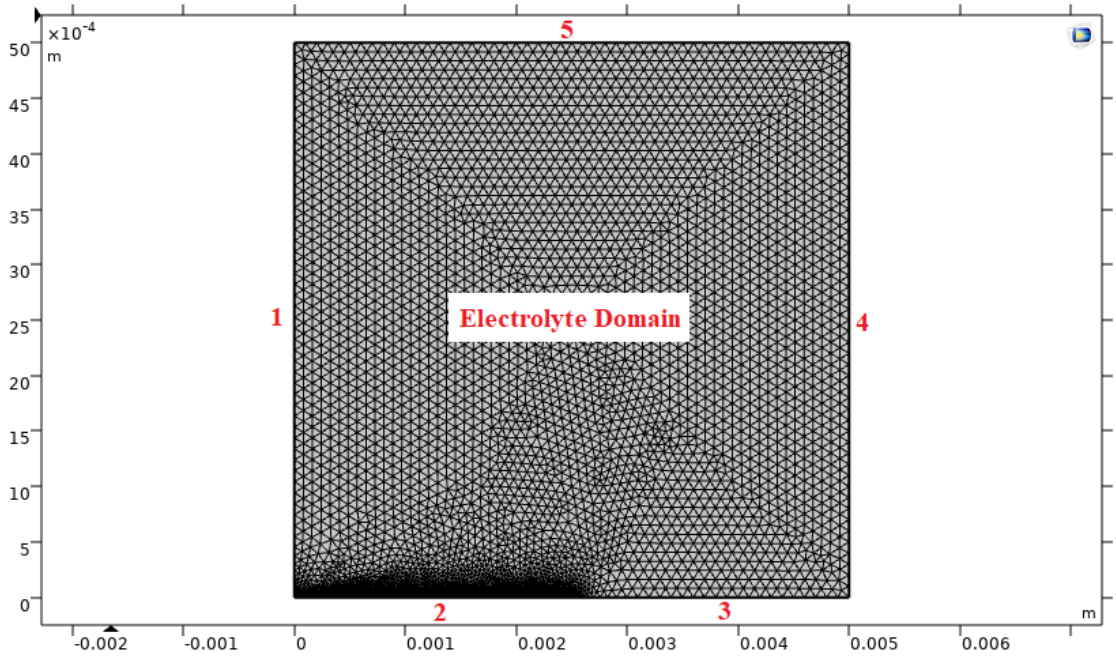

Figure 4.2. Schematic 2D meshed geometry in COMSOL Multiphysics.

Table 4.5. Parameter table.

Name	Value	Description
L1	5mm	Electrolyte domain thickness
L2	5mm	Electrolyte domain height
L3	2.5mm	Magnesium surface length
L4	2.5mm	Insulation tape length
sigma	16mS/cm	Electrolyte conductivity
Temp	298.15K	Temperature
R_gas	8.314J/mol/K	Gas constant
F	96485C/mol	Faraday's constant
pH	5.6	Electrolyte pH
pOH	8.4	Electrolyte pOH
i_corr (Mg353)	2.4866e-5A/cm^2	Corrosion current
E_corr (Mg353)	-1.2940V	Corrosion potential
i_corr (Mg403)	1.3564e-5A/cm^2	Corrosion current
E_corr (Mg403)	-1.2769V	Corrosion potential
i_corr (Mg503)	6.066e-6A/cm^2	Corrosion current
E_corr (Mg503)	-1.224V	Corrosion potential
Eeq_H	0.00V	E° for hydrogen half-cell reaction
Eeq_Mg	-2.372V	E° for magnesium half-cell reaction
Eeq_H2O	-0.8277V	E° for water half-cell reaction

4.4.3. Domain Conditions

Domain conditions are applied to the geometry domain to describe how the physics should be modelled throughout the entire domain. Some of the domain conditions for the Nernst-Planck Equations interface include Convection, Diffusion, and Migration as well as Initial Values and the charge numbers of the involved species. The modelled geometry, Figure 4.2, only has a single domain. Because general corrosion is assumed, the species considered within the domain are Mg^{2+}, H^+, OH^-, Na^+, and Cl^-. The initial values and the number of species are shown in the table below. The values in Table 4.1, Table 4.2, and Table 4.6 are used to describe the geometry domain.

Table 4.6. Initial values and charge numbers of the species.

Species	**Charge Number**	**Initial Concentration** ***(mol/m^3)***
Mg^{2+}	2	0
H^+	1	$10^{-5.6}$
OH^-	-1	$10^{-8.4}$
Na^+	1	154
Cl^-	-1	154

4.4.4. Boundary Conditions

The Nernst-Planck Equations interface has separate boundary conditions for the species concentrations and for the electric potential. This simply means that each boundary has two active boundary conditions. There are numerous possibilities for configuring the boundary conditions of the electric field and concentration fields, but not all configurations are significant or applicable. Table 4.7 shows the description of the boundary conditions.

Some of the species concentration boundary conditions include Concentration, Symmetry, Flux, and No Flux. The electrical potential boundary conditions include Current Density, Electrical Insulation, and Electrical Potential. The flux of a particular species calculated using Faraday's law is given as:

$$N_i = \frac{i_i}{z_i F} \tag{4.17}$$

N_i = the flux of the species *i*.
i_i = the current density of the species *i*.
z_i = the charge number of the species *i*.

The Tafel equation is utilised to determine the current density of different species involved in an electrochemical reaction. Equation (2.1) shows the Tafel equation for magnesium anodic oxidation reaction. The Tafel equations presented in equations (4.18), (4.19), and (4.20) are used to compute the fluxes associated with the anodic oxidation and cathodic reduction reactions in equations (2.1), (2.2), and (2.3) [48].

$$i_{Mg} = i_{0,Mg} \cdot exp\left(\frac{V - E^{\circ}_{Mg}}{\beta_{Mg}}\right) \quad (4.18)$$

$$i_{H} = - i_{0,H} \cdot exp\left(\frac{V - E^{\circ}_{H}}{\beta_{H}}\right) \quad (4.19)$$

$$i_{OH} = - i_{0,OH} \cdot exp\left(\frac{V - E^{\circ}_{OH}}{\beta_{OH}}\right) \quad (4.20)$$

i_{Mg} = the current density for magnesium oxidation reduction.

i_{H} = the current density for hydrogen reduction reaction.

i_{OH} = the current density for water reduction reaction.

$i_{0,Mg}$ = the exchange current density for magnesium.

$i_{0,H}$ = the exchange current density for hydrogen.

$i_{0,OH}$ = the exchange current density for water.

E°_{Mg} = the standard electrode potential for magnesium half-cell reaction.

E°_{H} = the standard electrode potential for hydrogen half-cell reaction.

E°_{OH} = the standard electrode potential for water half-cell reaction.

β_{Mg} = the Tafel constant for magnesium half-cell reaction.

β_{H} = the Tafel constant for hydrogen half-cell reaction.

β_{OH} = the Tafel constant for water half-cell reaction.

Table 4.7. Boundary conditions.

Species	**Species concentration BCs**			**Electric Potential BCs**
	Mg^{+2}	**H^{+}**	**OH^{-}**	
1	Symmetry	Symmetry	Symmetry	Electric Insulation
2	Flux	Flux	Flux	Current Density
3	No Flux	No Flux	No Flux	Electric Insulation
4	No Flux	No Flux	No Flux	Electric Insulation
5	Concentration	Concentration	Concentration	Electric Potential

The Nernst-Planck Equations Interface is used to obtain the concentration profile of the various chemical species in a physiological environment in the current work.

PART 5

RESULT AND DISCUSSIONS

5.1. TAFEL PLOTS AND DATA TABLE FROM EXPERIMENT

The potentiodynamic polarisation test is one of the most used direct current (DC) electrochemical techniques in evaluating the corrosion behaviour of metallic materials. This technique involves the application of a small potential to the working electrode, then varied linearly over a range of values. This results in the metallic surface oxidising or reducing because of the oxidation or reduction reactions. As the potential is varied, the current is measured and plotted as a function of the applied potential. The obtained plot is referred to as a polarisation curve.

There are two regions on the polarisation curve obtained from the experiments: the anodic and cathodic regions. The current response in the former is primarily due to oxidation reactions occurring at the electrode's surface, whereas the current response in the latter is primarily due to reduction reactions at the electrode's surface. Several important parameters that give insight into the behaviour of a metallic material such as corrosion current (I_corr) and corrosion potential (E_corr) can be extracted by analysing the polarisation curve. Figure 7 shows the potentiodynamic polarisation curves of the three samples used in this study in 0.9% Isotonic Sodium Chloride Solution (0.9% NaCl).

The corrosion resistance of sample Mg503 was superior to that of the other samples, as indicated by its lowest corrosion current value. Conversely, sample Mg353 exhibited the poorest corrosion resistance, as shown by its highest corrosion current value. Sample Mg403 demonstrated a corrosion resistance that was between sample Mg503 and sample Mg353. Table 5.1 provides data representation of the various

parameters and the corrosion rates obtained using the ASTM standard formula, equation 3.1, for the samples analysed in this study.

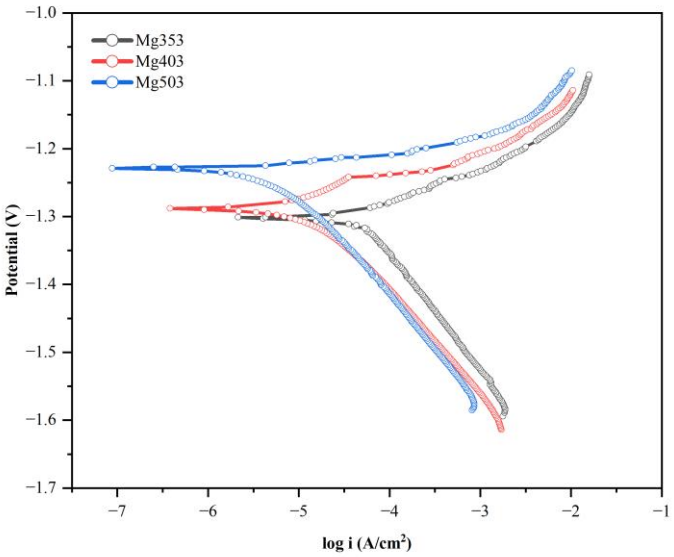

Figure 5.1. Potentiodynamic polarisation curves for AT31 alloys.

Table 5.1. Potentiodynamic polarisation experimental results.

Sample	**Corrosion Potential *(V)***	**Corrosion Current *(A/cm²)***	**Corrosion Rate *(mm/yr.)***
Mg353	-1.2940	2.4866e-5	0.5728
Mg403	-1.2769	1.3564e-5	0.3123
Mg503	-1.224	6.066e-6	0.1398

5.2. ELECTROLYTE POTENTIAL PLOTS FROM SIMULATION

Electrolyte potential refers to the electric potential or voltage difference that develops across an electrolyte solution. It basically indicates the potential that is generated due to ionic and electron movement/transfer within the electrolyte solution. It is a fundamental parameter that can be used for predicting the behaviour of an electrochemical cell and corrosion processes. When a solid electrode is submerged in an electrolyte solution, a potential difference arises from the transfer of electrons and ionic species, species such as Mg^{2+}, H^{+}, Na^{+}, Cl^{-}, OH^{-} etc. The species also play a crucial role in the generation of electrolyte potential.

Figure 5.2 shows the electrolyte potential plots for the three samples (Mg353, Mg403, and 503) at two extreme applied potential (voltage) values. The samples display negative electrolyte potentials at low potentials and positive electrolyte potentials at high potentials. Higher electrolyte potentials are observed close to the surfaces of the working electrodes and vary along the electrolyte domain. Electrochemical reactions occurring at the interface between the electrode and the electrolyte, and the species concentration gradient are some of the factors that contribute to higher electrolyte potentials near the electrode surfaces. Metals possessing a higher electrolyte potential tend to exhibit a greater tendency to oxidise easily, thereby leading to corrosion. Such metals are susceptible to corrosion, making them less corrosion resistant. On the other hand, a lower electrolyte potential corresponds to increased corrosion resistance. In the current study, sample Mg353 exhibits the highest electrolyte potential making it more corrosive than the other samples. Sample Mg503 exhibits the lowest electrolyte potential in comparison to the two samples, Mg353 and Mg403, making it the least corrosive sample. Sample Mg403 is less corrosive than sample Mg353 but more corrosive than sample Mg503 as indicated by its electrolyte potential values.

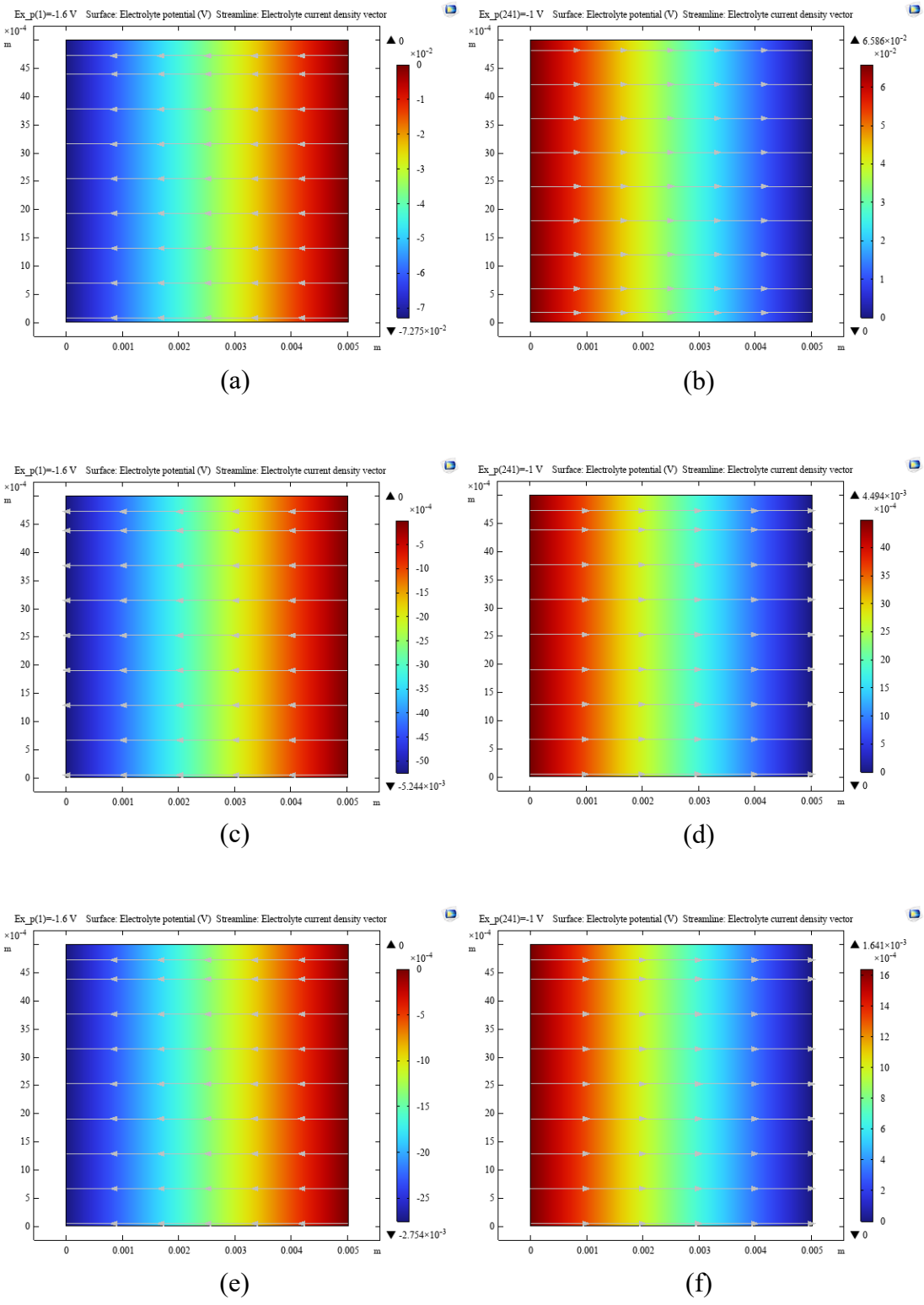

Figure 5.2. Electrolyte potentials for the three samples at two extreme applied voltages. Sample Mg353 (a, b), sample Mg403 (c, d), and sample Mg503 (e, f).

5.3. ELECTROLYTE CURRENT DENSITY PLOTS FROM SIMULATION

Another fundamental parameter used to predict the behaviour of an electrochemical cell and corrosion processes is electrolyte current density. It provides valuable information about the distribution and magnitude of the electric current density within the electrolyte solution. The movement of ionic species such as Mg^{2+}, Na^{+}, Cl^{-}, H^{+} etc., in the electrolyte solution facilitates the flow of electric current.

Figure 5.3 shows the electrolyte current density magnitude contour plots for the three different samples at one extreme applied potential value. The magnitude of the electrolyte current density is the same within the domain of the electrolyte solution. When the electrolyte current density is high, it implies that a large amount of current is passing through the electrolyte solution. Increased electrolyte current density signifies an accelerated corrosion process, and the opposite is true. In this study, the electrolyte current density magnitude for sample Mg353 is the highest compared to sample Mg403 and sample Mg503, making it more susceptible to corrosion than the other two samples. Sample Mg403 has an electrolyte current density magnitude that is between sample Mg353 and sample Mg503, making its corrosive behaviour less active in comparison to sample Mg353. The lowest electrolyte current density magnitude is exhibited by sample Mg503, making it the most corrosion-resistant sample among the three.

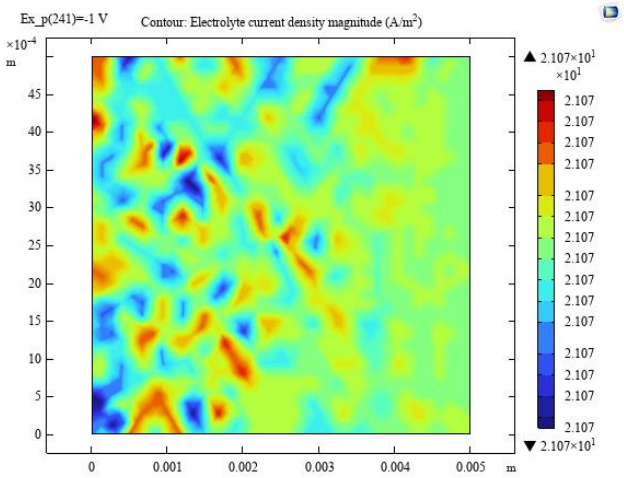

(a)

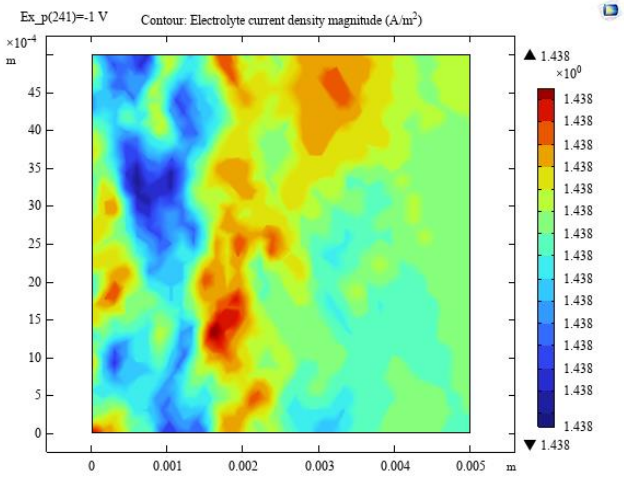

(b)

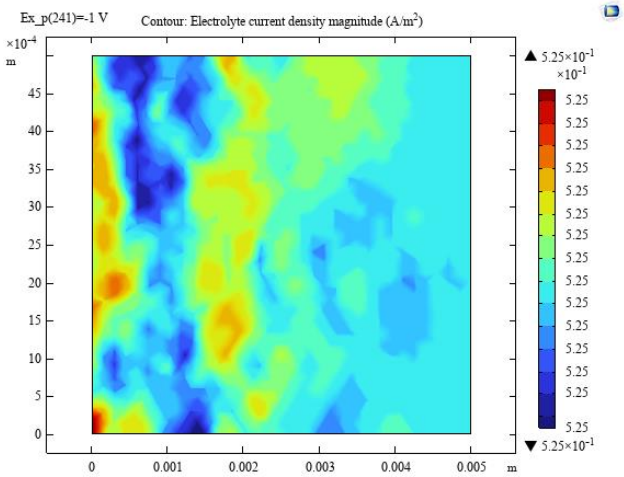

(c)

Figure 5.3. Electrolyte current density magnitude for the three samples at a single extreme applied voltage. Sample Mg353 (a), sample Mg403 (d), and sample Mg503 (c).

5.4. Mg^{2+} ION CONCENTRATION DISTRIBUTION PROFILE PLOTS FROM SIMULATION

The ionic species concentration distribution profile plots are obtained using the Nernst-Planck Equations Interface described in Chapter 4. The obtained results shown in the plots are purely based on the parameters used and obtained from the experiments. The ionic concentration distribution profile plots in this section provide information about the spatial distribution of Mg^{2+} ions within the electrolyte solution. The presence of a higher Mg^{2+} ion concentration in the electrolyte solution indicates an increase in the corrosion of magnesium whereas a lower Mg^{2+} concentration indicates a decrease in the corrosion of magnesium.

Figure 5.4 shows the Mg^{2+} ion concentration distribution profile plots for the three magnesium samples: Mg353, Mg403, and Mg503. The distribution of Mg^{2+} ions for the three samples is highest at the electrode/electrolyte interface and gradually decreases within the electrolyte solution. The Mg^{2+} ion concentration is highest for sample Mg353 indicating that the sample undergoes corrosion faster than the other samples. Sample Mg403 has reduced (Mg^{2+}) ion concentration over sample Mg353, making it less corrosive than sample Mg353. Nevertheless, sample Mg503 has the least magnesium (Mg^{2+}) ion concentration indicating that it undergoes corrosion slower than the sample Mg353 and Mg403.

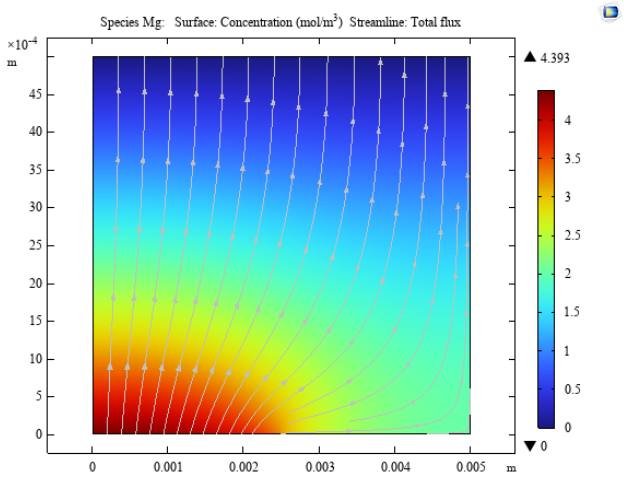

(a)

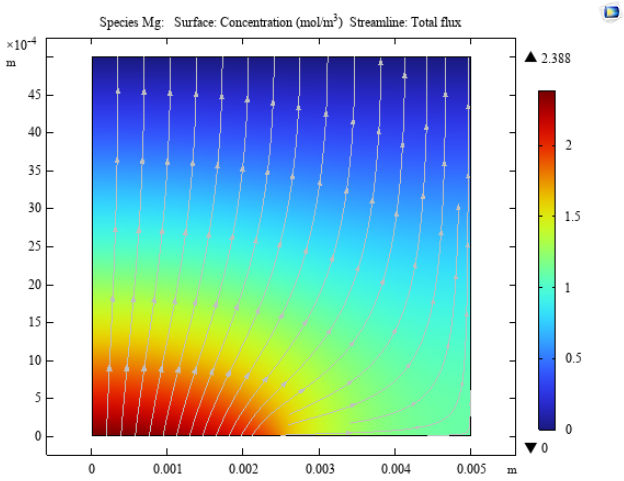

(b)

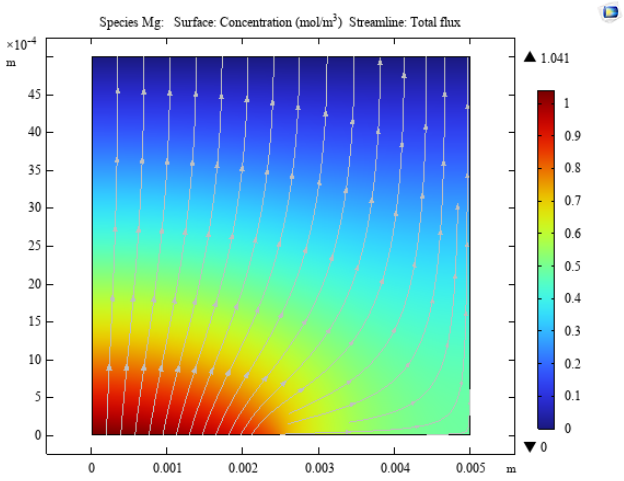

(c)

Figure 5.4. Magnesium ion concentration distribution profile for the three samples. Sample Mg353 (a), sample Mg403 (d), and sample Mg503 (c).

5.5. OH^- ION CONCENTRATION DISTRIBUTION PROFILE PLOTS FROM SIMULATION

The ionic concentration distribution profile plots in this section provide information about the spatial distribution of hydroxide ions (OH^-) within the electrolyte solution. The plots show that for each magnesium sample, the hydroxide ion concentration is at its peak at the magnesium surface and gradually diminishes on the electrolyte surface. The presence of the hydroxide ions is a result of the reduction reaction of water, as indicated by equation (2.3).

The OH^- ion concentration for sample Mg503 is the lowest, then that of sample Mg403, and finally that of sample Mg353, as indicated by Figure 5.5. The reduction of hydroxide ion concentration may be a good sign for corrosion; however, additional research is required to comprehend the correlation between the decrease in hydroxide ions and the corrosion of magnesium. According to the literature, a stable film of magnesium hydroxide – $Mg(OH)_2$, formed on the surface of magnesium effectively shields it from corrosion. It is worth noting that magnesium ions exhibit limited solubility, resulting in their precipitation as magnesium hydroxide. However, the limited solubility of magnesium ions (Mg^{2+}) does not necessarily affect the present study because steady-state magnesium corrosion is considered. The reaction quotient (Q_{sp}), governing the formation of magnesium hydroxide remains below the solubility product (K_{sp}), thus no precipitate is formed.

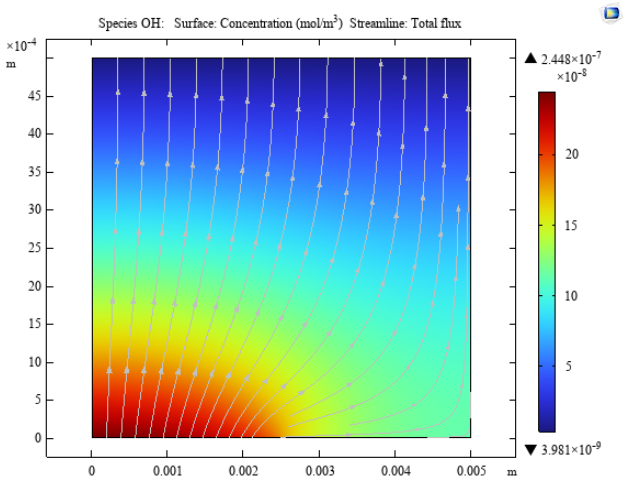

(a)

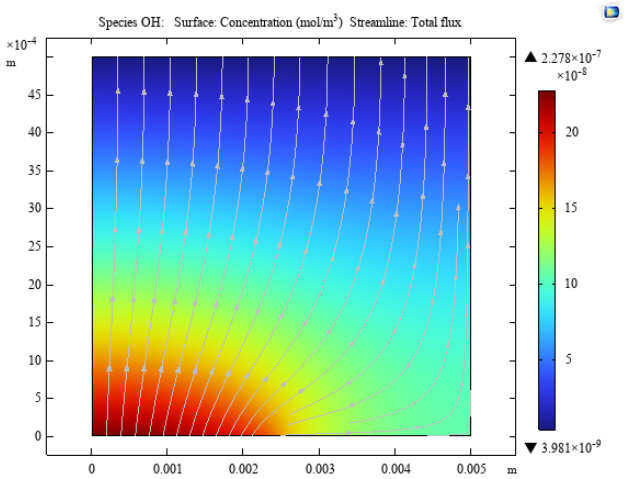

(b)

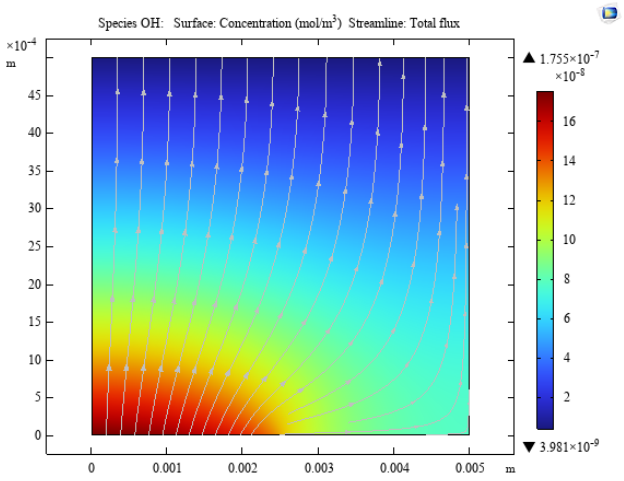

(c)

Figure 5.5. Hydroxide ion concentration distribution profile for the three samples. Sample Mg353 (a), sample Mg403 (d), and sample Mg503 (c).

5.6. WEIGHT LOSS ANALYSIS PLOT

Figure 5.5 shows the data obtained from the corrosion immersion test for weight loss measurements. Weight loss analysis was performed on the three samples, Mg353, Mg403, and Mg503, to further determine their corrosion behaviour. In this study, the total immersion method was utilised for weight loss measurements. The corrosive environment that was considered in this method was the 0.9% NaCl solution at 37 °C. The samples were immersed in the corrosive environment over a period of 7 days with weight loss measurements taken on the first day, third day, and the final day. It was observed that after three days all the samples exhibited a stable decrease in their weight loss as can be seen in Figure 5.6 below. After 7 days, sample Mg353 showed a drastic decrease in weight loss. On the other hand, samples Mg403 and Mg503 still maintained a steady decrease in their weight loss. The total measured weight loss over a period of 7 days for sample Mg353, sample Mg403, and sample Mg503 each decreased by 5.72%, 1.40% and 1.25% respectively. From the obtained weight loss measurements, sample Mg353 exhibited poor corrosion resistance compared to the other two samples. Sample Mg403 exhibited moderate corrosion resistance whereas sample Mg503 exhibited better corrosion resistance.

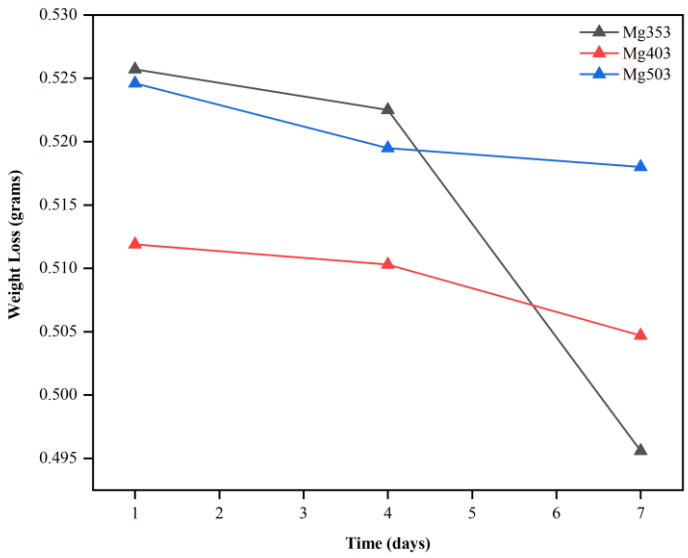

Figure 5.6. Weight loss measurements from corrosion immersion test for the three samples, Mg353, Mg403, and Mg503.

(a) (b) (c)

Figure 5.7. Samples after the immersion test. Sample Mg353 (a), sample Mg403 (d), and sample Mg503 (c).

PART 6

CONCLUSION AND FUTURE WORKS

6.1. CONCLUSION

The entire objective of this work was to compare the three AT31 magnesium alloys (Mg353, Mg403, and Mg503) regarding their corrosion behaviour in a physiological corrosive environment (0.9% NaCl) as well as evaluate the effectiveness of the simulation methods for verifying the experimental findings related to their corrosion performance. The simulation methods were demonstrated with simple models for studying the electrochemical corrosion behaviour of magnesium AT31 alloys. Electrochemical parameters such as corrosion current, corrosion potential etc., and other known parameters such as electrolyte conductivity, initial concentrations for various species, diffusion coefficients etc., were used to perform the simulations in COMSOL Multiphysics.

The simulated polarization curves exhibited the same trend as the experimental polarization curve. Figure 6.1 shows both the experimental and simulated polarisation curves. The corrosion current values obtained from the simulation for the three samples are shown in Table 6.1. These values together with equation 3.1 were used to calculate the corrosion rate of each sample. The corrosion rate values for the samples obtained from the experiment and the simulation are displayed in Table 6.1. As shown in the table, sample Mg503 has the lowest value for simulated corrosion current, meaning it possesses better corrosion resistance than the other two samples – its corrosion rate value also makes it apparent. On the other hand, the simulated corrosion current value for sample Mg353 is the highest in comparison to the other two samples, this indicates that it has the worst corrosion resistance, thus having a high corrosion rate. Additionally, sample Mg403 exhibited moderate corrosion resistance in comparison to the other samples. Figure 6.2 shows a plot for both experimental and

simulated corrosion rates. The simulated corrosion rates are higher than the experimental corrosion rates as expected, this is due to the assumptions that were considered for these simulations – see Chapter 4.

Literature suggests that one of the effective approaches to mitigate magnesium corrosion involves minimizing the release of Mg^{2+} ions and H_2 gases, as well as promoting a gradual generation of OH^- ions [29]. The reduction of hydroxide ion concentration may be a good sign for corrosion because higher levels of OH− ions will lead to surface alkalization and potentially damage cells around the implant. By observing the ion concentration distribution profile plots in Figure 5.4 and Figure 5.5, it can be concluded that with a decrease in the concentration of magnesium and hydroxide ions, magnesium corrosion decreases.

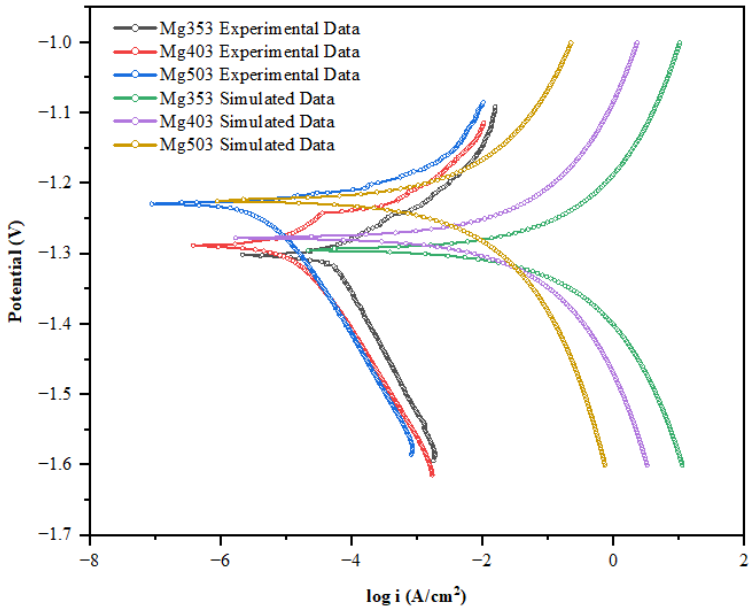

Figure 6.1. Experimental and simulated potentiodynamic polarisation curves for AT31 alloys.

Table 0.1. Corrosion current and corrosion rate summary table.

Sample	Experimental Corrosion Current – I_{corr} *(A/cm²)*	Simulated Corrosion Current – I_{corr} *(A/cm²)*	Experimental Corrosion Rate – CR *(mm/yr.)*	Simulated Corrosion Rate – CR *(mm/yr.)*
Mg353	2.487e-5	4.076e-5	0.5728	0.9388
Mg403	1.356e-5	2.154e-5	0.3123	0.4961
Mg503	6.066e-6	1.162e-5	0.1398	0.2676

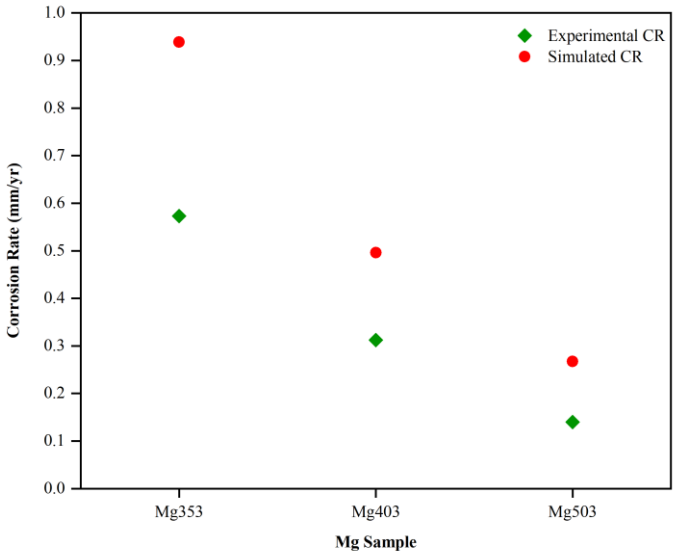

Figure 6.2. Experimental and simulated corrosion rate plot.

6.2. IMPLICATIONS OF THE RESULTS

- The results showed that Mg503 had the best corrosion resistance compared to Mg403 and Mg353. This suggests that hot rolling at higher temperatures can lead to grain refinement which in turn may improve the corrosion resistance of a material.
- Further comprehensive comparative studies of Mg AT31 alloy with other biodegradable materials (alloys) used for implant design must be performed in order for us to have a conclusive understanding of the use of Mg AT31 Alloys for medical implants.

6.3. FUTURE WORKS AND RECOMMENDATIONS

Some of the future works and recommendations to help fully understand the nature of Mg AT31 alloys are outlined below.

- Examine the mechanical integrity of the samples by conducting a destructive test – tensile test, of the three Mg AT31 alloys under two different conditions, (I; uncorroded samples – before corrosion tests, and (ii; corroded samples – after corrosion tests.
- Perform an ion concentration measurement test using an ion selective sensor for ionic species involved in corrosion Mg AT31 alloys and compare the measured test results to the simulated results.

REFERENCES

1. *International Grotto Directory*. (n.d.). https://osborne.house/profilego.asp?ref=2A3E39

2. Wikipedia contributors. (2023). Nehemiah Grew. *Wikipedia*. https://en.wikipedia.org/wiki/Nehemiah_Grew

3. *Joseph Black*. (n.d.). https://web.lemoyne.edu/~giunta/Black.html

4. Friend, J. N. (1950). The Discovery of Magnesium. *Nature*, *166*(4223), 615. https://doi.org/10.1038/166615b0

5. Durlach, J. (2007). Overview of Magnesium Research: History and Current Trends. In *Springer eBooks* (pp. 3–10). https://doi.org/10.1007/978-1-84628-483-0_1

6. Parida, P., Behera, A.K., & Mishra, S. (2012). Classification of Biomaterials used in Medicine. *International Journal of Advances in Applied Sciences, 1*, 125-129.

7. Radha, R., and D. Sreekanth. Insight of magnesium alloys and composites for orthopedic implant applications-a review. *Journal of Magnesium and Alloys* 5.3 (2017): 286-312.

8. Goodman, S.B., et al. The future of biologic coatings for orthopaedic implants. *Biomaterials* 34.13 (2013): 3174-3183.

9. H an, X., & Pan, J. (2013). Finite element analysis of degradation of biodegradable medical devices. *OA Biotechnology*, *2*(3). https://doi.org/10.13172/2052-0069-2-3-874

10. Witte, F., Ulrich, H., Rudert, M., & Willbold, E. (2007). Biodegradable magnesium scaffolds: Part 1: Appropriate inflammatory response. *Journal of Biomedical Materials Research Part A*, *81A* (3), 748–756. https://doi.org/10.1002/jbm.a.31170

11. Ambrose, C. G., & Clanton, T. L. (2004). Bioabsorbable Implants: Review of Clinical Experience in Orthopedic Surgery. *Annals of Biomedical Engineering*, *32*(1), 171–177. https://doi.org/10.1023/b:abme.0000007802.59936.fc

12. Song, G. (2007). Control of biodegradation of biocompatable magnesium alloys. *Corrosion Science*, *49*(4), 1696–1701. https://doi.org/10.1016/j.corsci.2007.01.001

13. Groenendijk, I., Van Delft, M., Versloot, P., Van Loon, L. J. C., & De Groot, C. (2022). Impact of magnesium on bone health in older adults: A systematic review

and meta-analysis. *Bone*, *154*, 116233. https://doi.org/10.1016/j.bone.2021.116233

14. Alawi, A. M. A., Majoni, S. W., & Falhammar, H. (2018). Magnesium and Human Health: Perspectives and Research Directions. *International Journal of Endocrinology*, *2018*, 1–17. https://doi.org/10.1155/2018/9041694

15. Staiger, M. P., Pietak, A., Huadmai, J., & Dias, G. J. (2006). Magnesium and its alloys as orthopedic biomaterials: A review. *Biomaterials*, *27*(9), 1728–1734. https://doi.org/10.1016/j.biomaterials.2005.10.003

16. Raffa, M. L., Nguyen, V., Hernigou, P., Flouzat-Lachaniette, C., & Haiat, G. (2020). Stress shielding at the bone-implant interface: Influence of surface roughness and of the bone-implant contact ratio. *Journal of Orthopaedic Research*, *39*(6), 1174–1183. https://doi.org/10.1002/jor.24840

17. Witte, F. (2010). The history of biodegradable magnesium implants: A review☆. *Acta Biomaterialia*, *6*(5), 1680–1692. https://doi.org/10.1016/j.actbio.2010.02.028

18. Biocompatibility and degradation study of magnesium alloys: a review. *International Journal of Emerging Technologies and Innovative Research* (www.jetir.org), ISSN:2349-5162, Vol.4, Issue 6, page no.526-536, June 2017, Available: http://www.jetir.org/papers/JETIR1706099.pdf

19. El-Rahman, S. S. A. (2003). Neuropathology of aluminum toxicity in rats (glutamate and GABA impairment). *Pharmacological Research*, *47*(3), 189–194. https://doi.org/10.1016/s1043-6618(02)00336-5

20. Witte, F., Hort, N., Vogt, C., Cohen, S., Kainer, K. U., Willumeit, R., & Feyerabend, F. (2008). Degradable biomaterials based on magnesium corrosion. *Current Opinion in Solid State & Materials Science*, *12*(5–6), 63–72. https://doi.org/10.1016/j.cossms.2009.04.001

21. Olanipekun, A. T., Faola, A. E., Oluwabunmi, K. E., & Oladosu, T. L. (2014). Galvanic Corrosion of a Mild Steel Bolt In A Magnesium Alloy (AZ91D) Plate Simulation Using Comsol Multiphysics. *International Journal of Scientific & Engineering Research*, *Volume 5*, 4.

22. Al-Shemmary, B. R., Matloub, F. K., & Al-Fetlawi, H. (2021). Modelling and Simulation of Pitting Corrosion. *Journal of Mechanical Engineering Research and Developments*, *Vol. 44*(No. 5), 10–17.

22. Gupta, D., Kumar, Y., Prajapati, V. *et al.* Time Dependent Analysis of Galvanic Corrosion on Mild Steel with Magnesium Alloy (AE44) Rivet-Plate Joint System Using COMSOL Multiphysics Simulation. *J Bio Tribo Corros* **8**, 111 (2022). https://doi.org/10.1007/s40735-022-00710-z

24. Cui, C., Ma, R. & Martínez-Pañeda, E. Electro-chemo-mechanical phase field modeling of localized corrosion: theory and COMSOL

implementation. *Engineering with Computers* (2023). https://doi.org/10.1007/s00366-023-01833-8

25. "Electrochemistry Module User's Guide, version 5.4", COMSOL, Inc, www.comsol.com

26. "Chemical Reaction Engineering Module User's Guide, version 5.4", COMSOL, Inc, www.comsol.com

27. *0.9% Sodium Chloride Injection, USP*. (n.d.). https://dailymed.nlm.nih.gov/dailymed/fda/fdaDrugXsl.cfm?setid=a4edf2d5-a9ff-30d4-e053-2995a90a5650&type=display

28. Reddi, B. (2013). Why Is Saline So Acidic (and Does It Really Matter?). *International Journal of Medical Sciences*, *10*(6), 747–750. https://doi.org/10.7150/ijms.5868

29. Song, G., & Song, S. (2007). A Possible Biodegradable Magnesium Implant Material. *Advanced Engineering Materials*, *9*(4), 298–302. https://doi.org/10.1002/adem.200600252

30. Zheng, Y. H., Gu, X., & Witte, F. (2014). Biodegradable metals. *Materials Science and Engineering R*, *77*, 1–34. https://doi.org/10.1016/j.mser.2014.01.001

31. Song, G., & Atrens, A. (2003). Understanding Magnesium Corrosion—A Framework for Improved Alloy Performance. *Advanced Engineering Materials*, *5*(12), 837–858. https://doi.org/10.1002/adem.200310405

32. Heublein, B., R, R., Kaese, V., Niemeyer, M., Hartung, W., & Haverich, A. (2003). Biocorrosion of magnesium alloys: a new principle in cardiovascular implant technology? *British Heart Journal*, *89*(6), 651–656. https://doi.org/10.1136/heart.89.6.651

33. Witte, F., Hort, N., Vogt, C., Cohen, S., Kainer, K. U., Willumeit, R., & Feyerabend, F. (2008). Degradable biomaterials based on magnesium corrosion. *Current Opinion in Solid State & Materials Science*, *12*(5–6), 63–72. https://doi.org/10.1016/j.cossms.2009.04.001

34. Gu, X., & Zheng, Y. (2010). A review on magnesium alloys as biodegradable materials. *Frontiers of Materials Science in China*, *4*(2), 111–115. https://doi.org/10.1007/s11706-010-0024-1

35. Agarwal, S., Curtin, J. F., Duffy, B., & Jaiswal, S. (2016). Biodegradable magnesium alloys for orthopaedic applications: A review on corrosion, biocompatibility and surface modifications. *Materials Science and Engineering: C*, *68*, 948–963. https://doi.org/10.1016/j.msec.2016.06.020

36. Pietak, A., Mahoney, P., Dias, G. J., & Staiger, M. P. (2007). Bone-like matrix formation on magnesium and magnesium alloys. *Journal of Materials Science: Materials in Medicine*, *19*(1), 407–415. https://doi.org/10.1007/s10856-007-3172-9

37. Dopp, E., & Rettenmeier, A. W. (2013). *Tin, Toxicity. In Springer eBooks (pp. 2235–2239).* https://doi.org/10.1007/978-1-4614-1533-6_118

38. Zhang, H., Feng, J., Zhu, W., Liu, C., Xu, S., Shao, P., Wu, D., Yang, W., & Gu, J. (2000). Chronic Toxicity of Rare-Earth Elements on Human Beings : Implications of Blood Biochemical Indices in REE-high Regions, South Jiangxi. *Biological Trace Element Research*, *73*(1), 1–18. https://doi.org/10.1385/bter:73:1:1

39. Kumar, K. S., Gill, R. S., & Batra, U. (2017). Challenges and opportunities for biodegradable magnesium alloy implants. *Materials Technology*, *33*(2), 153–172. https://doi.org/10.1080/10667857.2017.1377973\

40. Yun, Y., Dong, Z., Lee, N., Liu, Y., Xue, D., Guo, X., Kuhlmann, J., Doepke, A., Halsall, H. B., Heineman, W. R., Sundaramurthy, S., Schulz, M. J., Yin, Z., Shanov, V., Hurd, D., Nagy, P. B., Li, W., & Fox, C. A. (2009). Revolutionizing biodegradable metals. *Materials Today*, *12*(10), 22–32. https://doi.org/10.1016/s1369-7021(09)70273-1

41. Ropp, R. (2013). Group 16 (O, S, Se, Te) Alkaline Earth Compounds. In *Elsevier eBooks* (pp. 105–197). https://doi.org/10.1016/b978-0-444-59550-8.00003-x

42. Al-Gburi, A.S.N. (2022). *THE INVESTIGATION OF BIODEGRADABLE CORROSION PROPERTIES OF HOT ROLLED AT31 MG ALLOYS* (Publication No. 744268) [master's thesis, Karabük University] Ulusal Tez Merkezi.

43. Ali, I. (2022). *THE MICROSTRUCTURE AND MECHANICAL PROPERTIES OF HOT ROLLED AT31 MG ALLOYS MODIFIED BY LA AND GD* (Publication No. 719780) [master's thesis, Karabük University] Ulusal Tez Merkezi.

44. Gamry Instruments. (n.d.). *Potentiostat/Galvanostat Electrochemical Instrument Basics Gamry Instruments*. https://www.gamry.com/application-notes/instrumentation/potentiostat-fundamentals/

45. ASTM. (2015) *Standard Calculation of Corrosion Rates and Related Information from Electrochemical Measurements*, *G102-89. ASTM International.* vol. 3, no. 2.

46. Peng, J., Ji, G., Shi, Z., & Wang, X. (2021). Numerical Simulation Based on a ZrO2-Coated Stainless-Steel Corrosion Experiment. *ACS Omega*, *6*(22), 14504–14517. https://doi.org/10.1021/acsomega.1c01461

47. Samson, E., Marchand, J., & Snyder, K. A. (2003). Calculation of ionic diffusion coefficients on the basis of migration test results. *Materials and Structures / Matériaux Et Constructions*, *Vol. 36*(No. 257), 156–165.

48. N. Lee, "Corrosion Analysis of Biodegradable Magnesium Implants", M.S. thesis, School of Dynamic Systems, Univ. of Cincinnati, OH, 2009.

CURRICULUM VITEA

Bupe KASANYA completed his secondary education in the capital city of Zambia, Lusaka, after which he was awarded a scholarship by the Higher Education Loans and Scholarship Board (at the time, Bursaries Committee) to pursue his tertiary education in Turkey. He got accepted into the Faculty of Engineering at the University of Turkish Aeronautical Association to study in the Department of Mechanical Engineering, in 2013. The university granted him a full tuition fee waiver scholarship. He graduated with a Bachelor of Science (BS) degree in Mechanical Engineering in 2019. During his last B.Sc. year, he worked as an injection and trim machine operator at Endosa. In the summer of 2020, he got accepted to pursue a master's program in the Faculty of Engineering at Karabuk University to study in the Department of Metallurgical and Materials Engineering. Towards the end of his first year, he started working at Polimak as a Content Developer and is currently working as a Mechanical Engineer under the Research and Development Department (R&D). He graduated in 2023 with a Master of Science degree (MS) in Metallurgical and Materials Engineering.

CONFERENCES AND PUBLICATIONS:

Bupe K. (2023). FEM STUDY OF BIOCORROSION MG ALLOY FOR BIOMEDICAL IMPLANTS. Paper presented at the 4th Baskent International Conference on Multidisciplinary Studies held online and in-person on 4th to 6th August 2023 in Ankara, Türkiye.

Bupe K. (2023). FEM STUDY OF BIOCORROSION MG ALLOY FOR BIOMEDICAL IMPLANTS. Paper published in the 4th Baskent International Conference on Multidisciplinary Studies conference book on 10th September 2023.